Investigating c-Met Signaling in Non-Small Cell Lung Cancer

by

Cassandra L. Henry

BA, Ohio Wesleyan University, 2007

Submitted to the Graduate Faculty of

The School of Medicine in partial fulfillment

of the requirements for the degree of

Master of Science

University of Pittsburgh

2012

UNIVERSITY OF PITTSBURGH

SCHOOL OF MEDICINE

This thesis was presented

by

Cassandra Henry

It was defended on

April 24, 2012

and approved by

Marie C. DeFrances, M.D., Ph.D.

Associate Professor, Department of Pathology

Lin Zhang, Ph.D.

Associate Professor, Department of Pharmacology and Chemical Biology

Qiming Jane Wang, Ph.D.

Associate Professor, Vice Chair of Regulatory Affairs

Department of Pharmacology and Chemical Biology

Thesis Advisor: Jill M. Siegfried, Ph.D.

Professor and UPMC Chair, Department of Pharmacology & Chemical Biology

Investigating c-Met Signaling in Non-Small Cell Lung Cancer

Cassandra Henry, M.S.

University of Pittsburgh, 2012

Despite improvements in preventive, diagnostic, and therapeutic approaches, lung cancer remains the leading cause of cancer-related deaths in the U.S. There are currently no effective therapies for those diagnosed with later stage lung cancer. Recent efforts have focused on targeting specific lung cancer-related growth pathways, such as the hepatocyte growth factor (HGF)/c-Met signaling pathway. HGF/c-Met signaling plays a critical role in mediating proliferation, angiogenesis, invasion, and inflammatory responses in non-small cell lung cancer (NSCLC). This signaling pathway also confers resistance to therapies targeting other growth factor pathways such as epidermal growth factor receptor (EGFR) and vascular endothelial growth factor (VEGF). This study focuses on two aspects of HGF/c-Met signaling relevant to lung cancer: HGF stimulated c-Met angiogenic response and EGFR ligand-induced c-Met pro-cancer signaling. We previously reported airway expression of a human HGF transgene (HGF TG) produced mice that were more susceptible to lung tumorigenesis induced by a tobacco carcinogen. Here we show untreated HGF TG mice display enhanced vascularization and lymph vessel formation in the lungs compared to wild-type (WT) littermates, as ascertained by microvessel density. Whole lung microarray analysis consistently found significant decreases in expression of genes involved in angiogenesis including the VEGF family of genes (*Vegfa,Vegfb, Vegfc, Vegfd/Figf*) at 10, 20, and 40 weeks of age in HGF TG animals compared to WT littermates. HGF TG lung tumors derived from carcinogen treated HGF TG mice demonstrated

reduction in VEGF genes with an increased expression of five Cxcl family genes including *Cxcl1* and *Cxcl2* (murine forms of IL-8). Thus, increased vascularization produced by airway over-expression of HGF may occur through direct activation of c-Met on endothelial cells and expression of inflammatory mediators, rather than induction of VEGF pathways. Ligand-independent delayed and prolonged activation of c-Met has also been demonstrated previously by our laboratory via cross-talk from the EGFR pathway. Here we show that prolonged activation of STAT3 by EGFR-ligands is dependent on delayed c-Met activation. Inhibition of c-Met, by PHA665752, eliminates EGFR stimulated activation of STAT3 at delayed time points. The failure of Src inhibition, by PP2, to block delayed phospho-STAT3, and the co-immunoprecipitation of STAT3 with c-Met 8-24hours post EGF stimulation, suggests STAT3 is directly activated by c-Met. These data reinforce the idea that delayed c-Met activation is utilized by EGFR to potentiate its full biological effects through STAT3. Both ligand-dependent transient and ligand-independent delayed c-Met activation appear to be important in lung tumorigenesis. The findings of this study support future development of novel HGF/c-Met and EGFR combination therapies in NSCLC.

TABLE OF CONTENTS

LIST OF TABLES

LIST OF FIGURES

PREFACE

I would like to thank everyone from the Siegfried Laboratory for his or her input, guidance, and continuing support. I'd especially like to thank Mary Rothstein for her assistance with the mouse experimentation. I owe my deepest gratitude to Dr. Laura Stabile. From direct assistance on animal experimentation to general guidance, I am extremely appreciative of her involvement in all aspects of my project. I'd also like to thank Dr. Ariel Lopez-Chavez for his technical and intellectual assistance concerning the HGF/c-Met angiogenic studies.

I am indebted to my thesis advisor, Dr. Jill Siegfried. Her guidance and support through some of my most trying times will never be forgotten. I am also grateful to each of the members of my thesis committee for their assistance and support towards seeing me graduate.

Finally I give an extra-special thank you to my family and friends. To my fellow students, who have enhanced my experience tremendously, I will fondly remember our adventures. To my parents and siblings for their everlasting love and encouragement, and Joe for never failing to brighten my mood, thank you.

1.0 INTRODUCTION

1.1 LUNG CANCER STATISTICS AND RISK FACTORS

Lung cancer is the leading cause of cancer related deaths in the United States and worldwide (1). Though incidence rates have started to decline (1.9% decrease per year in men, 0.3% in women), there is still an estimated 226,160 new cases of lung cancer expected in 2012 (2). Lung cancer deaths will account for 28% of all cancer related deaths this year alone. The five-year survival rate has remained largely unchanged at only 16% for decades. The rate is 52% when the cancer is detected while still localized, but only 15% of cases are diagnosed at this early a stage (2). Thus, despite the decreased number of cases each year due to decreasing risk factors such as cigarette smoking, new lung cancer cases are often diagnosed at late stages when effective therapeutic options are few.

Exposure to tobacco by means of cigarette, pipe, or cigar smoke remains the greatest risk factor for lung tumorigenesis accounting for 90% of all cases (2). In 2009, 23.5% of men and 17.9% of women in the United States smoked, with the greatest prevalence in the 25-44 year old age group (24.0%) (3). There are currently over one billion smokers worldwide, with four-fifths of those in low or middle-income countries (3). It is estimated that tobacco related deaths will increase to 8.3 million by 2030, with 80% of deaths occurring in developing countries (4).

Other risk factors include: exposure to radon gas released from soil and building materials, exposure to secondhand smoke, asbestos, arsenic, chromates, and generalized air pollution (2, 5). Gender differences have been reported to play a role in the development of lung tumors. Nearly 80% of lung cancer in the non-smoking population occurs in females (3). The observed sex differences may be due to several factors including differences in environmental exposures (6) or steroid hormones, such as the estrogen receptor family (7), increasing susceptibility to lung cancer development and progression.

Two basic pathological classifications are used to describe lung cancer: small cell lung cancer (SCLC) and non-small cell lung cancer (NSCLC). NSCLC accounts for nearly 85% of all lung carcinomas, and generally grows more slowly than SCLC (1). NSCLC can be further divided by histology into subtypes including adenocarcinoma (35%), large cell carcinoma (<10%), and squamous cell carcinoma (25%). Tumors that are classified by cytological appearance provide oncologists with characteristics that allow for more effective treatment.

1.2 DIAGNOSIS AND THERAPIES

Lung cancer is often undiagnosed until late stages of the disease (IIIB, IV). This can be attributed partially to the fact that early stages of the disease tend to be asymptomatic. There are also no formal guidelines in place for early screening. The National Lung Screening Trial recently compared two methods of detecting lung cancer: low-dose helical computed tomography (CT) and standard chest X-ray. Results from this study revealed that patients who received CT scans had a lower mortality rate than those who received standard chest X-rays (8). However, potential risks associated with radiation exposure from multiple CT scans have not been evaluated.

Treatments, based on type and stage of cancer, include radiation therapy, surgery, chemotherapy, and targeted therapies (2). The treatment choice for early-stage lung cancer, surgical resection, focuses on removing as much of the tumor as possible without damaging adjacent tissue. Chemotherapy treatment destroys rapidly proliferating cells, and thus is the usual treatment choice for SCLC. Chemotherapy and/or radiotherapy for late-stage NSCLC offer only short-term survival benefits (9). Recent research has demonstrated a potential for targeted drugs in advanced-stage NSCLC patients especially when combined with chemotherapy treatments.

1.3 GROWTH FACTOR SIGNAING IN LUNG CANCER

Escape from normal control pathways is a key event in the development of lung cancer. Following the discovery of epidermal growth factor (EGF), a multitude of secreted factors that control key pathways such as cell proliferation, survival, and metastasis have been identified (10). These pathways are often deregulated in malignancies (11). Growth factors act through autocrine and paracrine mechanisms but cannot cross the cell membrane. Instead, they often bind cell surface receptors that possess intrinsic tyrosine kinase activity. Abnormalities, by means of mutation or expression deregulation, have been reported in many cancers, including NSCLC (12). Thus, these molecules may serve as valuable targets for therapy. Current FDA approved targeted therapy in NSCLC is limited to inhibition of the EGFR and vascular endothelial growth factor (VEGF) pathways.

1.3.1 Mediators of Angiogenesis

Several growth factors mediate angiogenesis, the formation of new blood vessels from pre-existing vasculature, which plays a crucial role in the development and continuation of tumor progression. Microvessel density is often utilized to quantify angiogenic activity (13, 14). Several studies have demonstrated an association between increased microvessel density and poor patient outcomes in NSCLC (14-16). The inhibition of angiogenesis is expected to prevent growth and emergence of tumor progression (17). So far, bevacizumab is the only approved anti-angiogenic agent for NSCLC. The combination of bevacizumab with carboplatin/paclitaxel was approved for first-line treatment of patients with NSCLC in 2006 (18).

Bevacizumab is a humanized monoclonal antibody that binds and inhibits all members of the VEGF family. VEGF is largely considered the key regulator in the promotion of endothelial cell proliferation and vascular permeability (12). Early studies indentified VEGF as a significant prognostic factor in NSCLC (18). Reports of resistance to these anti-VEGF treatments have been reported in several types of cancer, including NSCLC (17, 19). Recent evidence suggests other pathways such as interleukins, platelet-derived growth factor (PDGF), fibroblast growth factor (FGF), and hepatocyte growth factor (HGF) are sufficient for signaling that promotes angiogenesis (20). Levels of HGF and other pro-angiogenic cytokines have been reported to be elevated before progression in colorectal cancer patients being treated with bevacizumab (21).

Tobacco smoke, an important risk factor for lung carcinoma, is an irritant that induces the release of pro-inflammatory cytokines, chemokines and reactive oxygen species (22). Several genes associated with the promotion of inflammation have also been shown to play important roles in the promotion of angiogenesis (e.g. KRAS, TNFα, Interleukins) (23). Interleukin 6 (IL-6) and interleukin 8 (IL-8) are CXC chemokines that act as chemoattractants for neutrophils and

macrophages, as well as stimulate proliferation of endothelial and lung tumor cells (24). The CXC family of chemokines are heparin-binding molecules that contain four conserved cysteine residues (25). These chemokines are subdivided into ELR+ and ELR- depending on the presence (+) or absence (-) of a Glu-Leu-Arg tripeptide motif immediately preceding the first cysteine on the NH3 terminus (Table 1). ELR+ CXC chemokines are angiogenic, whereas ELR- CXC chemokines are angiostatic (24, 26). CXC receptor type 2, which mediates angiogenic effects, is located on neutrophils, endothelial cells, and tumor cells (27-29). A recent study in CXCR2 deficient mice demonstrated its signaling is required for tumor growth and angiogenesis regardless of the presence of VEGF (30). Similarly, inhibition of IL-8 via a neutralizing antibody reduced tumorigenesis of NSCLC in SCID mice (31). Other studies have also determined CXC chemokines are important for the promotion of angiogenesis in patients with NSCLC (32, 33) and have reported IL-8 as a proliferative factor for NSCLC cells (34-36).

Table 1. Angiogenic chemokine ligands and receptors (Strieter, RM, *et al.* 2008).

Systematic Nomenclature	Old Nomenclature	Receptor
Angiogenic/arteriogenic		
CXCL1	Gro-α	CXCR2
CXCL2	Gro-β	CXCR2
CXCL3	Gro-γ	CXCR2
CXCL5	ENA-78	CXCR2
CXCL6	GCP-2	CXCR2
CXCL7	NAP-2	CXCR2
CXCL8	IL-8	CXCR2
CCL2	MCP-1	CCR2
CCL11	Eotaxin	CCR3
CCL16	HCC-4/LEC	CCR1
Angiostatic		
CXCL4, CXCL4L1	PF-4, PF-4_{var}	CXCR3B*
CXCL9	Mig	CXCR3B
CXCL10	IP-10	CXCR3B
CXCL11	I-TAC	CXCR3B

Growth factors other than VEGF, such as HGF, have been reported to stimulate induction and release of these ELR+ CXC chemokines (37). HGF, which will be discussed in greater detail later, activates integrins on endothelial cells to trigger development of the lymphatic vessels (22), and triggers macrophages to release cytokines such as IL-8 (24). HGF has also been shown to directly promote blood vessel formation during tissue repair that does not require VEGFs (38). Recently, it has been documented that HGF/c-Met activation also plays a role in resistance to sunitinib treatment, a VEGFR and PDGFR inhibitor (19).

Epidermal growth factor is yet another growth factor pathway known to play a role in the regulation of angiogenesis (18). Dual inhibition of VEGFR and EGFR by vandetanib has been shown to demonstrate anti-tumor activity. Yet, significant survival benefits were not demonstrated in Phase III clinical trials for NSCLC patients (39).

1.3.2 Epidermal Growth Factor Receptor

Thus far, the most promising inhibition of NSCLC via growth factor blockade has come from obstruction of the EGFR signaling pathway. The EGFR family has been studied as a target for anticancer therapies in NSCLC for over a decade since the first EGFR-mutant lung cancers were described (40, 41). While normal epithelial cells express EGFR, it is over-expressed in up to 60% of NSCLC tumors (42). When activated via interaction with its ligands EGF, transforming growth factor-alpha (TGFα), and amphiregulin (AR), EGFR can form homodimers or heterodimers with the other monomers of the EGFR family HER2, HER3, or HER4 (43, 44). Dimerization is crucial for trans-autophosphorylation within the intracellular tyrosine kinase domain. This is followed by subsequent downstream phosphorylation of the carboxy-terminal

tail. These phosphorylated residues serve as the site for interaction with adaptor proteins. The adapter proteins in turn modify effector molecules such as RAS/mitogen-activated protein kinase (MAPK), phosphatidylinositol 3-kinase (PI3K)/Akt, and signal transducer and activator of transcription (STAT) proteins, which promote cell proliferation, motility, and invasion (45).

In order to block EGFR hyper-activation in NSCLC, tyrosine kinase inhibitors (TKIs) and monoclonal antibodies were designed. Cetuximab (brand name: Erbitux), a chimeric monoclonal antibody, and panitumumab (brand name: Vectibix), a human monoclonal antibody, bind to the extracellular domain of EGFR preventing natural ligand-induced phosphorylation and subsequent intracellular signaling. Phase III trials have shown conflicting results using cetuximab in chemotherapy-naïve patients regarding overall survival (46). However, when combined with chemotherapy clinical outcomes were improved (46, 47). Additional data is required before these antibodies can be approved for treatment of NSCLC.

In 2003 and 2004 the first EGFR TKIs, gefitinib (brand name: Iressa) and erlotinib (brand name: Tarceva) were approved for the treatment of advanced NSCLC. Both are orally available quinazoline-based molecules that reversibly compete with ATP to inhibit kinase activity (48). Both drugs seemed promising in cell and animal models, but had decreased clinical efficacy due to resistance. It was determined that patients harboring EGFR mutations benefited from EGFR TKIs compared to those with wild-type EGFR. EGFR mutations occur in only 26% of NSCLC tumors. This incidence increases to 77% among EGFR TKIs responders (46).

Despite positive responses to EGFR TKIs, most patients develop resistance within a year (46). Resistance can be acquired or intrinsic. Intrinsic resistance is important in NSCLC patients expressing wild-type EGFR, which account for the majority of NSCLC cases (49). Secondary mutations in EGFR can confer resistance to TKIs. The T790M mutation is found in 50% of

patients that relapse after initial response to EGFR TKIs (48). This mutation is thought to block EGFR TKI binding but still allow binding of ATP. Other genomic alterations can induce primary resistance to EGFR inhibitors, such as activating mutations in downstream signaling transducers. KRAS mutations, predominately in codons 12 and 13, occur in 15-20% of lung cancer patients and are correlated with poor prognosis (50). These activating mutations occur in molecules downstream of receptor activation, thus continuing to drive tumor formation regardless of receptor status (49). Divergence to other signal transduction pathways may also confer resistance to EGFR inhibition. Redundancy among receptor tyrosine kinases (RTKs) allows for the activation of overlapping signaling cascades to continually stimulate effector molecules involved in tumor progression. One such pathway, HGF/c-Met, has been demonstrated to be important for EGFR resistance in NSCLC. The amplification of c-Met allows for continued activation of mediators such as PI3K and MAPK in the presence of EGFR inhibitors (46, 51). Amplified c-Met combined with the T790M mutation accounts for 70% of acquired EGFR TKI resistance in NSCLC (46). Thus, there is a strong basis for exploring the c-Met signaling pathway as a therapeutic target in NSCLC.

1.4 HEPATOCYTE GROWTH FACTOR AND C-MET

1.4.1 HGF and c-Met Structure

The MET proto-oncogene encodes a transmembrane receptor with tyrosine kinase activity. The 150kDa precursor is glycosylated to become a fully mature 170kDa pro form of c-Met. This pro-molecule is then cleaved into two subunits, the α-chain (45kDa) and β-chain (150kDa). The

mature c-Met receptor is comprised of the two chains connected by a disulfide linkage. The β-chain forms the transmembrane portion of c-Met. Its intracellular segment contains the juxtamembrane and tyrosine kinase domains (Figure 1) (52). The extracellular section forms a binding pocket with the solely extracellular α-chain. It is here that the c-Met ligand, HGF, binds.

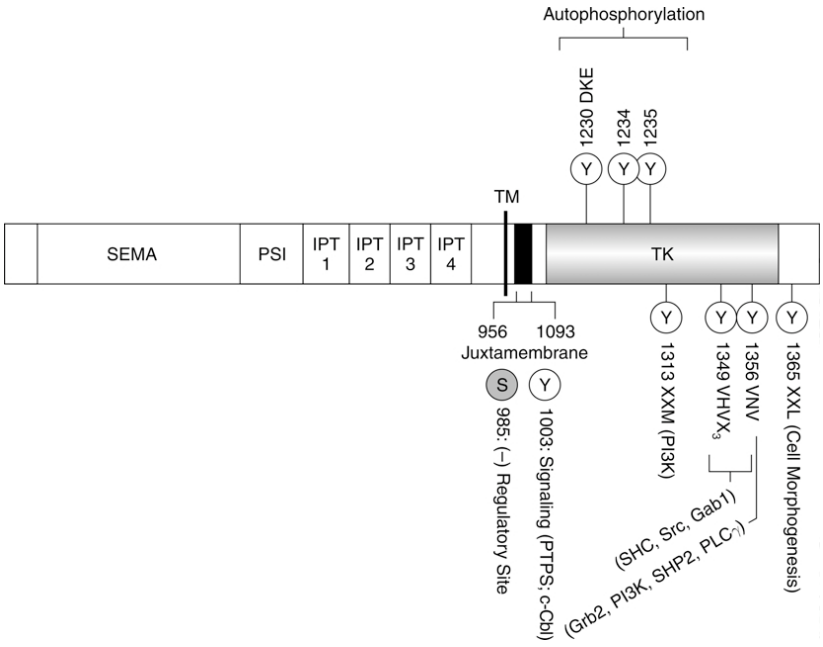

Figure 1. Structure of c-Met and important phosphorylation sites (Ma, PC, *et al.* 2003).

Cells of a mesenchymal origin, such as fibroblasts, secrete HGF. HGF was originally discovered as a platelet-derived mitogen for hepatocyte cells that induced epithelial cell scattering (53). It is secreted as an inactive pro-molecule, which is then activated via cleavage by serine proteases (Figure 2) (54). The mature form is composed of an α-chain and β-chain linked by a disulfide bridge. Functional HGF binds the c-Met receptor to initiate downstream signaling cascades.

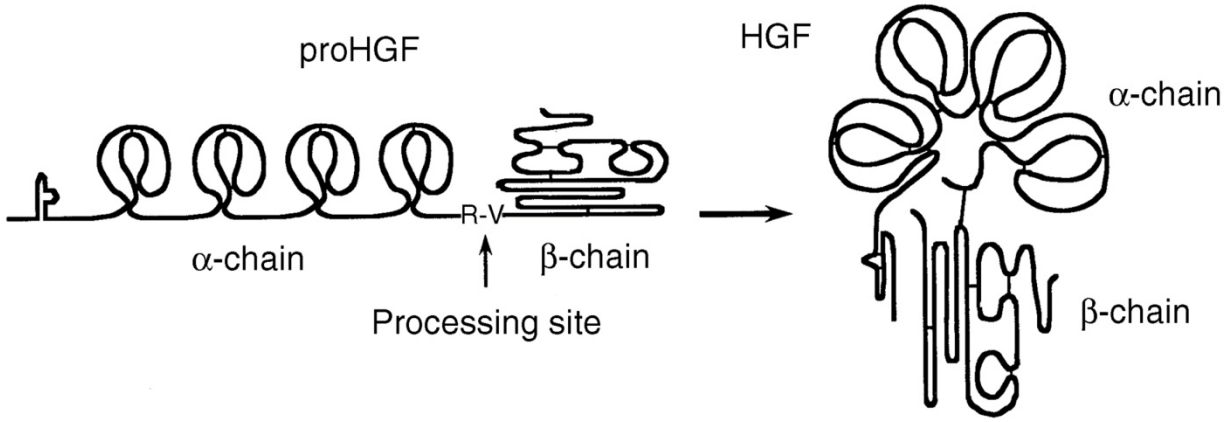

Figure 2. Structure of pro- and mature HGF (Matsumoto, K, *et al.* 2001).

1.4.2 HGF/c-Met Signaling

In the canonical pathway, binding of HGF facilitates the dimerization and autophosphorylation of key tyrosines in the β-chain of the c-Met receptor. Tyrosine residues Y1230, Y1234, and Y1235 are essential to the tyrosine kinase activity of c-Met. Phosphorylation at these sites leads to subsequent phosphorylation on tyrosine residues Y1349 and Y1356 (52). These form the multi-substrate docking site (MSDS), which is recognized by the majority of adaptor molecules that regulate downstream signaling such as c-Src, PI3K, Grb2, or GRB2-associated-binding protein 1 (Gab1) (Figure 2 and 3) (55). Protein-interactions occur through PTB, SH2, and met binding domains (MBD). Phosphorylation at residue Y1003 is recognized by

the E3 ubquitin ligase c-Cbl, which then plays a role in the ubiquitinization, internalization, and degradation of c-Met (Figure 2) (56).

HGF/c-Met activates several downstream signaling cascades, which modulate growth, motility, anti-apoptosis, inflammation, invasion, and angiogenesis (Figure 3). The Ras/MAPK cascade activates cell proliferation and growth (57). This pathway is stimulated in a rapid and transient manner. The STAT family of transcription factors, including STAT3, plays a key role in invasive phenotypes seen after HGF stimulation (58). HGF is also able to promote inflammation or angiogenesis by acting on macrophages or epithelial cells directly through c-Met receptors (59). Indirectly, HGF promotes angiogenesis and inflammation by stimulating the production of cytokines and chemokines including COX-2 (11), or IL-8 (37).

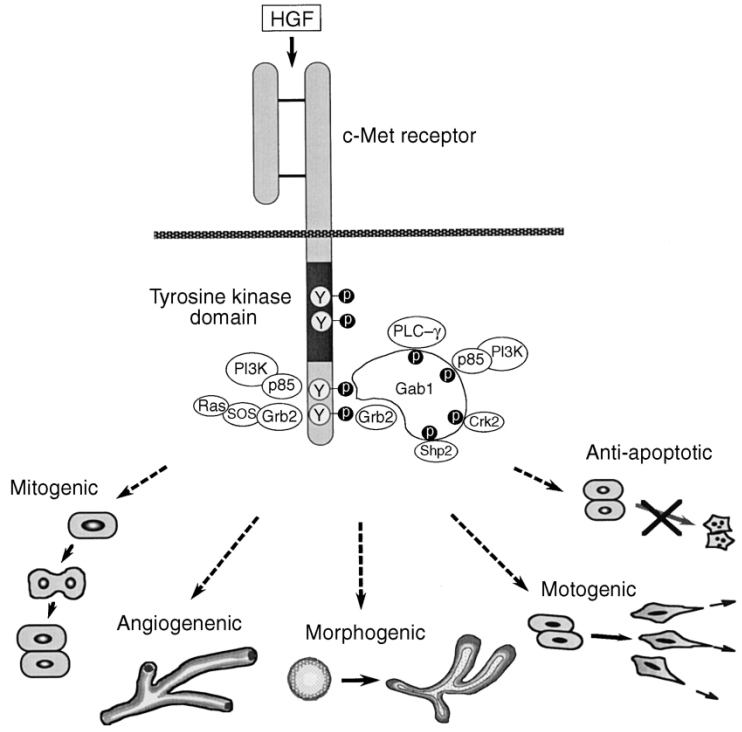

Figure 3. Canonical HGF/c-Met signal transduction pathway (Matsumoto, K, *et al.* 2001).

1.4.3 Function in Normal Tissues versus Cancer

In normal tissue, HGF/c-Met signaling is essential for embryonic development and tissue regeneration. This pathway is important for placenta and liver development during embryogenesis (60). HGF and c-Met knockout mice are both embryonically lethal (61). In adults signaling is transient and activated only during injury and repair processes (62). Following injury to heart, kidney, or liver, HGF plasma levels increase as secreted HGF from local and/or distant sites promote cell migration for the reconstitution of injured tissues (63-65). HGF levels decrease to basal conditions once regeneration is complete.

In cancer cells, this transient signaling is uncontrolled and up-regulated. Tumor stromal cells are the main source of HGF in NSCLC. HGF released from stromal cells acts in a paracrine mechanism on surrounding epithelial and endothelial cells (66). Over-expression of HGF and c-Met is present in approximately 50% of lung adenocarcinomas (67-69), and is strongly correlated with poor prognosis of NSCLC patients (70-72). An increased number of receptors can drive oligomerization of c-Met resulting in ligand-independent activation (73). In addition, mutations have been reported that cause the loss of Y1003, the residue involved in regulating internalization (74). This loss confers prolonged activation of the c-Met signaling cascade. Transient signaling in normal tissues makes HGF and c-Met ideal for targeting tumor cells.

1.4.4 C-Met Crosstalk and Delayed Activation

Although typical activation of c-Met occurs by HGF stimulation, c-Met may also be activated by ligand-independent means. Cell surface proteins that respond to extracellular signals have been shown to activate c-Met through crosstalk or lateral signaling. Proteins that act as c-

Met partners include integrins, CD44, class B plexins, G protein coupled receptors (GPCRs) and other RTKs such as RON and EGFR (75). The mechanism in which these molecules activate c-Met varies greatly. For example, integrin clustering triggers c-Met phosphorylation independent of HGF following cellular adhesion in mouse melanoma cells (76). While these associations are likely indirect, HGF-induced interaction of c-Met with the laminin receptor, α6β4, enhances phosphorylation of integrin β4 (75). Single-pass transmembrane plexins modulate cytoskeletal remodeling and integrin-dependent adhesion. Class B plexins share homology with c-Met in their extracellular domains, which allows for ligand-independent association. Activated c-Met has been associated with activated plexin B1 in carcinoma cells (77). Another transmembrane protein, CD44, can act as a co-receptor for c-Met, thus enhancing HGF-stimulated c-Met signaling (75). GPCR ligands such as lysophosphatidic acid (LPA), thrombin, and bradykinin are able to induce c-Met phosphorylation via ectodomain shedding (78). Here, loss of the extracellular fragment of c-Met allows for the intracellular portions to dimerize in the absence of ligand. Moreover, crosstalk may occur between c-Met and other RTKs, EGFR being the most well documented of these interactions.

EGFR and c-Met receptors are often co-expressed in tumors, including NSCLC. Activation of c-Met following stimulation with EGFR ligands has been observed in lung and epidermal carcinoma cells (79). Crosstalk from EGFR to c-Met occurs in the presence of mutant or wild-type EGFR, and correlates with receptor expression levels (75). Our laboratory previously demonstrated that invasion of NSCLC cell lines stimulated by prostaglandin E2 (PGE2) involves EGFR ligand production, which in turn leads to activation of EGFR and successive phosphorylation of c-Met (11). We further established that EGFR activation of c-Met in NSCLC cells is a delayed event that occurs through an intracellular signaling cascade

independently of HGF (80). Delayed lateral signaling from EGFR to c-Met is required to obtain the maximal invasive phenotypic response to EGFR ligand stimulation in NSCLC cells (80).

1.4.5 HGF/c-Met Pathway Therapeutics

HGF/c-Met inhibition by small molecule inhibitors, and antibodies targeted to HGF or c-Met has been shown to reduce tumorigenesis (53, 81, 82). These findings along with the knowledge that HGF/c-Met signaling confers resistance to EGFR TKIs, has spurred the development of therapeutic agents targeting the HGF/c-Met signal transduction pathway. HGF inhibitor and Met antagonist therapeutics function outside target cells. Monoclonal antibodies directed against HGF (AMG102), or the c-Met receptor (METMab), disrupt interactions between HGF and c-Met at the binding pocket (83). Biological antagonists, NK1, NK2, and NK4 are non-cleavable forms of HGF that bind Met without inducing receptor activation (84). While these therapies are currently under investigation, the majority of HGF/c-Met inhibitors are c-Met directed TKIs that function inside the cell (83, 84).

In the inactive conformation, an activation loop blocks ATP access to the c-Met catalytic domain. Upon activation, the loop is extruded and ATP binds a pocket between the N and C lobes (83). The c-Met kinase inhibitors fall under three groups depending on their mode of binding. Types I, II, and III are all ATP competitive inhibitors. Type I inhibitors, such as PHA665752 and PF02341066, display preferential binding to inactive c-Met proteins (83). Type II (BMS-777607) and Type III inhibitors also bind the ATP pocket but extend into other cavities of the receptor (83). The efficacies for these inhibitors are currently being evaluated with the majority in phase I or II clinical trials. The Met and ALK inhibitor, PF2341066, has shown high efficacy in patients with NSCLC containing activating ALK gene fusions or Met alterations (85).

A phase III clinical trial is ongoing for this compound with hopes that it will be used in lung tumors with the activating ALK fusion gene or c-Met amplification. While initial results from clinical studies have shown therapeutic benefits, larger and more rigorous trials will clarify the true value and long-term safety of these inhibitors in cancer patients.

1.4.6 HGF Transgenic Mouse

In order to effectively study HGF/c-Met signaling in lung tumorigenesis, our laboratory has generated and published the phenotype of a transgenic mouse over-expressing human HGF in the airways under the control of the Clara cell secretory protein (CCSP) promoter (86). This mouse expresses human HGF protein in CCSP-positive cells only and contains a 3.5-fold increased level of HGF in the BAL fluid. The transgenic animals do not spontaneously develop lung tumors. However, after exposure to the tobacco carcinogen 4-(methylnitrosoamino)-1-(3-pyridyl)-1-butanone (NNK), HGF TG mice exhibited a significant increase in tumor multiplicity compared to wild-type (WT) littermates (86). This effect of HGF over-expression was successfully blocked by 90% when using an HGF neutralizing antibody (82). NNK-induced tumors in HGF TG and WT littermates had an identical frequency of K-ras mutation of 40%, suggesting HGF promotes tumor development regardless of K-ras status. In the presence of HGF neutralizing antibody, tumors were more likely to be K-ras mutant when compared to a control neutralizing antibody (82); thus suggesting tumors containing mutant K-ras better survive the blockade of HGF/c-Met signaling. HGF TG mice were also observed to contain higher pulmonary blood vessel production after NNK exposure than their WT littermates. Few studies have been completed that further characterize vessel formation and gene expression changes in the presence of HGF over-expression.

1.5 FOCUS OF RESEARCH

The research undertaken for the Master's Degree focused on two aspects of HGF/c-Met signaling that are relevant to lung cancer.

1) Determine which genes are involved in the angiogenic response to HGF.
2) Understand how HGF-independent activation of c-Met downstream of EGFR contributes to pro-cancer signaling.

EGFR has been well established to play an important role in lung tumorigenesis. However, a lack of clinical efficacy, with c-Met signaling noted as a major factor of acquired resistance, has prompted us to explore unanswered questions about HGF/c-Met signaling in lung cancer. Upon further investigation, we will gain a better understanding of the critical intermediates involved in two differing c-Met signaling cascades; HGF-stimulated blood vessel formation, and EGFR ligand-induced c-Met invasion. This knowledge can be utilized for the clinical development of novel HGF/c-Met and EGFR combination therapies in NSCLC.

1.6 MATERIALS AND METHODS

1.6.1 Chemical Reagents

PHA665752 was obtained from Pfizer under an approved material transfer agreement (New York, NY). PP2 was purchased from Calbiochem (San Diego, CA). Gefitinib and Vandetanib were purchased from ChemieTek (Indianapolis, IN). EGF was purchased from Invitrogen (Carlsbad, CA). HGF was purchased from R&D Systems (Minneapolis, MN). The c-Met and

non-targeting siRNA ON-TARGET*plus* SMARTpools were purchased from Dharmacon (Lafayette, CO).

1.6.2 Cell Lines and Culture Conditions

H1435 NSCLC cell line was obtained from American Type Culture Collection (Manassas, VA). The 201T cell line was established in our laboratory from a primary lung adenocarcinoma (87). Cells were grown in Basal Medium Eagle (BME) or RPMI 1640 containing 10% fetal bovine serum and 2mM L-Glutamine. All cells were maintained at 37ºC in 5% CO_2. Cells were grown to 60-80% confluence in full serum medium and serum-deprived 48 hours prior to growth factor stimulation unless otherwise stated. DNA fingerprinting was used to verify the identity of each cell line.

1.6.3 Protein Analysis

Cellular Isolation and Cytosolic-Nuclear fractionation

Following experimental treatment, cells were washed twice with 1X phosphate-buffered saline (PBS) and lysed with NP-40 lysis buffer (50mM Tris-HCl, 150mM NaCl, 1% NP-40, pH 8.0) containing protease inhibitor cocktail (Roche, Indianapolis, IN) and phosphatase inhibitors: sodium fluoride (NaF, 25mM) and sodium orthovanadate (NaV, 1.5mM). After being briefly sonicated and incubated on ice for 30 minutes, the insoluble fraction was cleared by centrifugation at 10,000 x g for 20 min at 4ºC. To analyze subcellular localization of STAT3/pSTAT3, nuclear and cytoplasmic protein fractions were collected using Chemicon's

Nuclear Extraction Kit (Millipore, Billerica, MA), following manufacturer's instructions. The BCA-200 Protein Assay Kit (Pierce, Rockford, IL) was utilized for protein quantification.

Tissue Isolation

For extraction from tissue specimens, tissue sections were immediately frozen in liquid nitrogen upon removal. Lung samples were homogenized using a polytron (VWR VIDI 25) in 0.5mL ice-cold radioimmunoprecipitation assay (RIPA) buffer containing complete mini protease inhibitor cocktail tablet. Phenylmethylsulfonyl fluoride stock (0.2M) was added to each lysate and incubated on ice for 30 minutes. The insoluble fraction was cleared by centrifugation at 10,000 x g for 15 minutes at 4ºC. Protein was quantified using the BCA-200 Protein Assay Kit.

Immunoprecipitation

Equal amounts of protein were subjected to immunoprecipitation with indicated antibodies while rotating overnight at 4ºC. Lysates were then incubated with Protein A-Agarose Beads (Thermo Fisher Scientific, Rockford, IL) for 2 hours at 4ºC. Samples were washed 4X with NP-40 lysis buffer, followed by resuspension in 2X Laemmli sample buffer (2% SDS, 25% Glycerol, 62.5mM Tris-HCl pH 6.8, 0.01% Bromophenol Blue, 5% ß-mercaptoethanol).

Western Blotting

Equal amounts of protein (50μg) were separated on 7.5% or 10% SDS-Tricine gels under reducing conditions. Protein was transferred to nitrocellulose membrane before blocking with 5% milk or BSA, 1x Tris-Buffered Saline (TBS) with Tween 20. Membranes were incubated with primary antibodies in 3% milk or BSA, 1x TBST at 4ºC overnight. After primary antibody

incubation, blots were washed 3X with 1x TBST (10 minutes each at room temperature), and horseradish peroxidase-conjugated anti-mouse, anti-rabbit, or anti-goat IgG was added at a 1:2,000 dilution for 2 hours at room temperature. After washing another 3X with 1x TBST, immunoreactive peptides were visualized using SuperSignal West Pico Chemoluminescent substrate (Pierce) followed by exposure to autoradiography film. For re-probing, blots were stripped with Restore Western Blot (Thermo Fisher Scientific). Immunoreactive bands were quantified by densitometry and ImageQuant analysis.

Primary Antibodies

Primary Antibody	**Species; Dilution**	**Manufacturer**
Total c-Met (C-28)	Rabbit; 1:1000 (WB) 1:75 (IHC)	Santa Cruz Biotechnology (Santa Cruz, CA)
Phospho-c-Met (Y1234/35)	Rabbit; 1:1000	Cell Signaling (Beverly, MA)
Total c-Src	Mouse; 1:1000	Invitrogen
Phospho-STAT3 (Y705)	Rabbit; 1:1000	Cell Signaling
Total STAT3	Rabbit; 1:1000	Cell Signaling
Phospho-tyrosine (pY99)	Mouse; 1:750	Santa Cruz Biotechnology
β-Actin	Mouse; 1:5000	Sigma-Aldrich
Akt (C-20)	Rabbit; 1:1000	Santa Cruz Biotechnology
Vegfa (A-20)	Rabbit; 1:500	Santa Cruz Biotechnology
Vegfd (C-18)	Goat; 1:1000	Santa Cruz Biotechnology
PARP 1/2 (H-250)	Rabbit; 1:1000	Santa Cruz Biotechnology
LYVE-1	Rabbit; 1:100	Abcam (Cambridge, MA)
SMA (1A4)	Mouse; 1:50	R&D Systems
PECAM-1 (M-20)	Goat; 1:100	Santa Cruz Biotechnology

1.6.4 RNA Analysis

RNA Isolation

After experimental treatment, cells were washed on ice 2X with 1x PBS. Total RNA was extracted using the RNeasy Mini Kit (Qiagen, Valencia, CA) following the manufacturer's protocol. Briefly, cells were lysed with Buffer RLT, subjected to column purification, and resuspended in RNase free water. Tissue samples for gene expression analysis were stored in RNAlater (Qiagen) at -80ºC. Sections were weighed and homogenized in TRIzol (Invitrogen) followed by column purification via the Array Grade Total RNA Isolation Kit (SABiosciences, Frederick, MD) according to manufacturer's instructions. RNA was quantified using a Nanodrop 2000 spectrophotometer.

Reverse Transcription Polymerase Chain Reaction (RT-PCR)

Knockdown of c-Met by siRNA transfection was validated using RT-PCR. cDNA was synthesized and subjected to PCR using Qiagen's OneStep RT-PCR Kit. Each 50µl reaction contained 500ng total RNA, 12.5mM $MgCl_2$, 0.6µM of c-Met primers: forward (5'-CAACAGCACTGTTATTACTACTTGGG-3'), reverse (5'-GCACTTGTCGGCATGAACCG-3'). RT-PCR was completed in an automatic thermocycler under the following conditions: 30 minutes of reverse transcription at 50ºC, 15 minutes at 95ºC for Taq activation and denaturation, 25 cycles of 30 seconds denaturation at 94ºC, 30 seconds annealing at 58ºC, and 60 seconds extension at 72ºC, followed by 10 minutes at 72ºC for final extension. Twenty microliters of each reaction were run on a 1.5% agarose gel. Bands were quantified by densitometry.

Microarray Analysis

Total RNA extracted from whole lung or isolated tumors from HGF TG or WT mice was subjected to qPCR analysis (Angiogenesis PCR Array [PAMM-024], SABiosciences) or hybridization to Oligo GEArray Mouse Angiogenesis or Cancer Pathway Finder Microarrays (SuperArray OMM-44 and OMM-33, respectively). In both cases, cDNA was reverse transcribed from total RNA using RT^2 First Strand Kit (SABiosciences). cDNA was directly applied to the Angiogenesis PCR Array and qPCR was performed on ABI Prism 7700 Sequence Detector (Applied Biosystems, Foster City, CA). The threshold cycle (Ct) value of each gene was measured and expression analysis was completed using the RT2 Profiler PCR Array Data Analysis (www.sabiosciences.com). Prior to overnight hybridization to the Oligo GEArrays, cDNA was labeled with biotin-16 using the True-Labeling-AMP Linear RNA Amplication Kit (SABiosciences). Signal was detected via exposure to autoradiography film. Data analysis was performed using GEArray Expression Analysis Suite (www.sabiosciences.com). Data are presented as the relative induction of each gene normalized to housekeeping genes, and are representative of two to four independent experiments. These data have been deposited in the National Center for Biotechnology Information's Gene Expression Omnibus (GEO) and are accessible through GEO Series accession number GSE20468.

1.6.5 Mouse Models

For all experiments mice were either WT (murine HGF) or human HGF transgenic (FVB/N strain). Construction of the human HGF transgene, as well as generation and identification of HGF TG mice, was previously described (86).

Microarray Analysis

Whole lungs were dissected from untreated WT and HGF TG animals after sacrifice at 10, 20, or 40 weeks of age. To induce lung tumors, mice were given a total of four intraperitoneal injections of 3mg NNK (15mg/mL) over 2 weeks. NNK induced lung tumors were dissected from the animals at 20 or 40 weeks of age.

Growth Factor Inhibitors

WT and HGF TG mice (5 weeks of age) were treated with gefitinib (75mg/kg), vandetanib (25mg/kg), or vehicle control (1% Tween-80/0.9% saline). Treatment was administered by oral gavage (0.2mL/mouse) twice a week for five weeks. At the end of treatment, animals were sacrificed and lungs were inflated with 10% buffered formalin under 25cm intra-alveolar pressure and removed. Half of the lung was harvested for protein and RNA analysis; the other half was fixed in 10% formalin for immunohistochemical (IHC) analysis. Animal care was in strict compliance with the institutional guidelines.

1.6.6 Immunohistochemistry

Whole mouse lungs were fixed in 10% buffered formalin and stored in 100% ethanol. Tissues were then embedded in paraffin, sectioned, and mounted on slides. Slides were deparaffinized, rehydrated, and steamed in EDTA (pH 8.0) followed by 3% hydrogen peroxide at room temperature for antigen retrieval. To identify vessel expression of the c-Met receptor, slides were stained with anti-c-Met (C-28) for 1 hour. Antibody against PECAM-1 (M20, 1.5 hours) was used as a pan-endothelial marker. Staining of lymphatic vessels was accomplished with anti-LYVE-1 for 1 hour. H&E staining was also performed on serial sections from the same lung

specimens. Microvessels, as detected by PECAM-1, were counted in five WT mice per time point. Lymphatic vessels, as detected by LYVE-1, were counted in ten high-magnification areas per lung from six HGF TG and six WT mice at 20 weeks of age. Results are expressed as the mean number of blood vessels per area ± standard error.

1.6.7 Immunofluorescence

Dual immunofluorescence was utilized to distinguish the maturity of blood vessels. Whole lung samples were fixed in 10% formalin and stored in 100% ethanol. Tissues were embedded in paraffin, sliced, and mounted on slides. Slides were deparaffinized with xylenes, rehydrated, and subjected to antigen retrieval via heating in citrate buffer (pH 6.0) for ten minutes. After blocking with 10% normal serum in PBS with 2% BSA, slides were incubated overnight at 4ºC with a mixture of anti-PECAM (M20) and anti-smooth muscle actin (SMA) in PBS with 0.5% BSA. Slides were washed 3X with PBS-Tween 20 (PBST) five minutes each time. Secondary antibody incubation was performed in the dark with donkey anti-goat-546 and donkey anti-mouse-488 Alexa-fluorophore conjugated IgG (Invitrogen) at a dilution of 1:500 in 0.5% BSA for 1 hour at room temperature. Slides were washed another 3X with PBS and mounted with Vectasheild Fluorescence Mounting Medium (Vector Laboratories, Burlingame, CA). Vessels as detected by PECAM or SMA were counted in seven high-magnification areas per lung from six HGF TG and six WT mice at 20 weeks of age. Results are presented as the mean number of mature vessels per area (as stained by SMA), total blood vessels per area (as stained by PECAM), and percentage of SMA-positive vessels (SMA stained vessels/total vessels stained by PECAM) ± standard error.

1.6.8 siRNA Transfection

201T cells were transfected with 50pmol of either non-targeting or c-Met siRNA pools using Oligofectamine (Invitrogen) in serum free medium. After 8 hours, transfection medium was replaced with serum containing medium overnight followed by serum starvation and experimental treatment.

1.6.9 Statistical Analyses

All values were obtained using Student's t-test, except for the *in vivo* growth factor inhibitor experiment, for which a one-way ANOVA with Tukey post-test was utilized. All tests were two-sided with the threshold for significance defined as $P < 0.05$. For array analysis, adjusted p-values were calculated using the Benjamini Hochberg method. Comparisons that remained significant using this correction method are indicated with an asterisk within the tables.

2.0 HGF INDUCES PULMONARY VASCULARIZATION

2.1 INTRODUCTION

Lung cancer is the number one cause for cancer-related deaths in men and women in the United States, accounting for 15% of new cancer diagnoses and 28% of all cancer deaths (1). Therapeutic options for patients are limited and new approaches are necessary to improve prognosis. NSCLC accounts for more than 80% of all lung cancers, and is dependent on angiogenesis (88, 89). The inhibition of angiogenesis is expected to prevent both the growth of tumor cells and emergence of tumor progression, thereby improving the prognosis of patients with NSCLC (17). The VEGF pathway is considered one of the major regulators in angiogenesis in normal and malignant tissues (89). However, resistance to anti-VEGF therapies and a lack of substantial clinical benefit with such treatments has been reported in NSCLC (17, 19). Recent evidence suggests that other pathways such as interleukins and HGF/c-Met signaling are sufficient to promote angiogenesis (20, 90, 91).

While induction of VEGF in response to HGF has been reported, HGF has also been shown to induce neovascularization independently of VEGF (20, 92). For example, HGF-dependent signaling through c-Met expressed on lymphatic endothelial cells is known to directly promote blood vessel formation during tissue repair, and does not require VEGFs (93). HGF can activate integrins on endothelial cells to trigger development of the lymph vascular system with

endothelial cell proliferation, survival, and migration (92). HGF also activates macrophages, which express the c-Met protein; macrophages can trigger angiogenic processes through release of cytokines such as IL-8 (94).

In normal cells, c-Met activation is a transient event, whereas in tumor cells c-Met activity may be up-regulated by both receptor and ligand over-expression (68, 95). Over-expression of HGF and c-Met has been reported in nearly 50% of lung adenocarcinomas (67-69), and is a strong independent prognostic factor in various cancers including lung, breast, biliary tract, gastric, and nasopharyngeal carcinoma (70-72). The strong correlation between HGF/c-Met expression and patient survival, coupled with its limited effect on normal adult tissue processes, advocates HGF/c-Met signaling as a useful therapeutic target with few adverse effects.

To better understand the effects of HGF/c-Met signaling pathway in lung cancer, we previously generated transgenic mice with elevated HGF expression in the airway epithelium under the control of the Clara cell secretory protein promoter (86). We previously documented that when exposed to the tobacco carcinogen, NNK, the HGF TG mice exhibited a significant increase in tumor multiplicity compared to WT littermates (86). In that study, we observed high pulmonary blood vessel production in HGF TG mice after NNK exposure. Here we further characterize the vessel formation in HGF TG versus WT animals. Furthermore, to analyze which genes contribute to the differences in blood vessel formation, we profiled the expression of genes representative of pathways involved in angiogenesis and tumorigenesis using commercial microarrays from individual untreated lungs as well as from lung tumors that arose in NNK-treated HGF TG and WT mice.

2.2 RESULTS

2.2.1 HGF Over-expression Results in Enhanced Blood Vessel Formation.

H&E staining and PECAM immunohistochemistry were used to compare blood vessel density in the lungs of HGF TG and WT mice. Blood vessels, indicated by PECAM, were counted in five high-magnification areas per lung from HGF TG (n=5) and WT (n=5) mice at 10, 20, and 40 weeks of age. A considerable excess of blood vessels was observed by both H&E (Figure 4A and 4B) and PECAM (Figure 4C and 4D) staining in the lungs of HGF TG (Figure 4B and 4D) mice compared to WT littermates (Figure 4A and 4C). This increase in blood vessel production was consistently seen in the lungs of HGF TG mice at all time points (10-40 weeks). The ratio of TG:WT blood vessel density was calculated and shown to increase over time (Figure 4E). The maximal effect occurred at 40 weeks with more than a 4-fold increase in blood vessel density in HGF TG mice (24.6 ± 3.9 microvessels/area) compared to WT lungs (5.8 ± 1.6 microvessels/area, P=0.0022, Figure 4E).

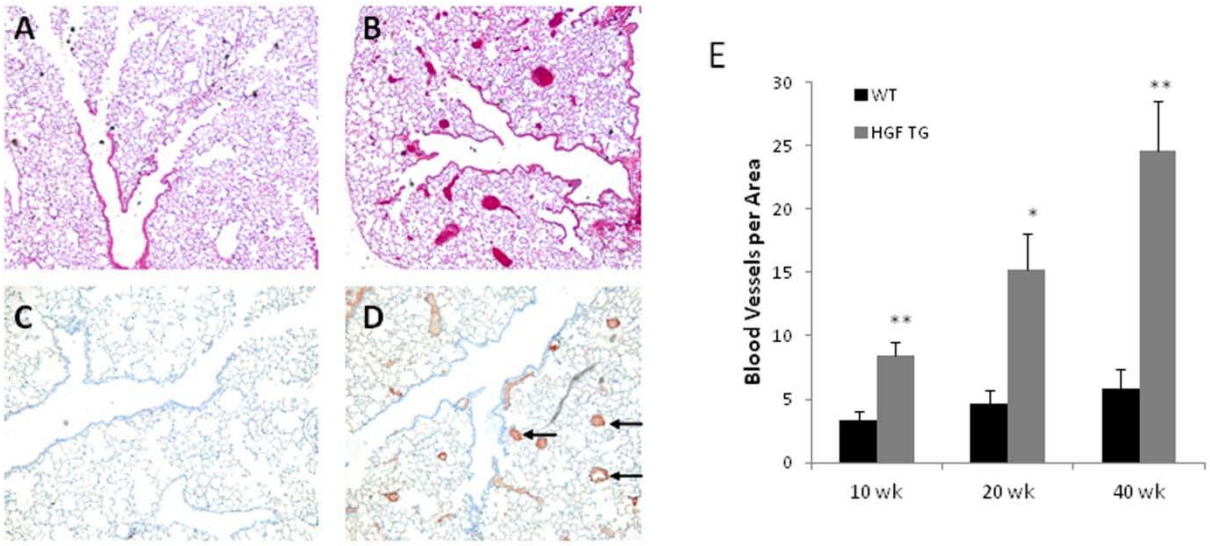

Figure 4. **Enhanced blood vessel formation in HGF TG mice vs. WT littermates.** Representative pictures from 20 wk old WT (A,C) and HGF TG (B,D) mouse lungs. **A,B**. H&E staining. **C,D.** PECAM immunohistochemistry. Arrows indicate areas of increased blood vessel formation. **E.** Average number of blood vessels ± standard error from 5 high-magnification areas per lung of 5 HGF TG and 5 WT mice per time point. Asterisk denotes level of significance of HGF TG to similarly aged WT mice (* <0.05, ** <0.005, *** <0.001)

2.2.2 Pulmonary Endothelial Cells Express c-Met Receptors.

Pulmonary endothelial cells in WT mice are known to express c-Met receptors. C-Met immunohistochemistry was performed to confirm c-Met expression by pulmonary vessel endothelial cells in transgenic mice. As expected, endothelial cells stained positive for c-Met in both WT and HGF TG lungs (Figure 5). There was no difference in the percentage of c-Met positive endothelial cells between HGF TG and WT lungs. C-Met staining in blood vessels of HGF TG animals did however appear more intense compared to the staining in WT vessels. This could be due to an increase in number of receptors in the HGF TG vessels. HGF has been

reported to up-regulate its own receptor (96). The expression of c-Met receptor in endothelial cells of both HGF TG and WT mice suggests these vessels are able to directly respond to HGF stimulation.

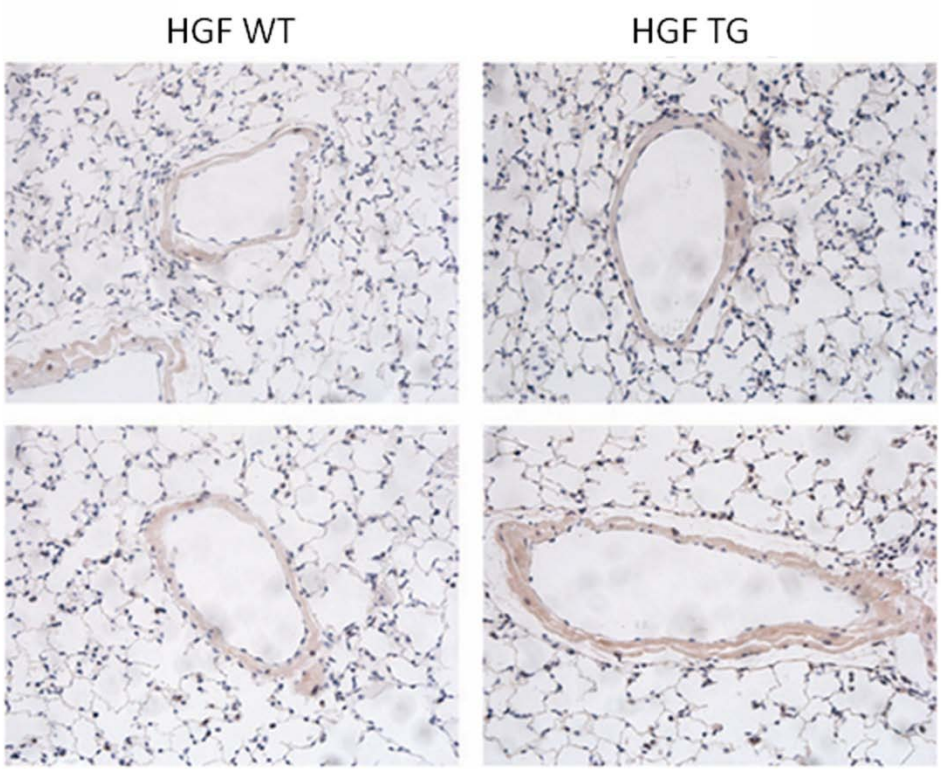

Figure 5. C-Met immunostaining. Representative pictures from WT and HGF TG mouse lungs. Endothelial cells in both HGF TG and WT mice stain positively for c-Met.

2.2.3 HGF Stimulated Vessels Show a Lesser Degree of Maturation.

The PECAM immunohistochemistry results suggest that HGF over-expression continuously stimulated microvessel formation as mice aged. To confirm this, the degree of vessel maturation was examined at an intermediate time point (20 weeks of age), when enhanced vessel growth was incomplete. Nascent endothelial tubes form prior to pericyte coverage (97). The acquisition of pericytes indicates vessel stabilization and maturation (97). PECAM, as a pan-endothelial marker, does not distinguish vessel maturity. Only mature, pericyte containing vessels stain positive with SMA, a pericyte marker (98, 99). Whole lungs from HGF TG (n=6) and WT (n=6) mice were dual stained with SMA and PECAM to determine the average number of mature vessels (WT=4.05 ± 1.43), TG=6.33 ± 1.54) and total vessels (WT=5.02 ± 1.72, TG=9.42 ± 1.86) per area. Representative images are shown in Figure 6A. The percentage of SMA positive vessels was determined by dividing the average number of SMA stained vessels by PECAM stained vessels in HGF TG and WT animals. A significantly smaller fraction of vessels stained positive for SMA in HGF TG mice (67 ± 1.8% SMA positive vessels) compared to WT littermates (80 ± 2.9% SMA positive vessels, P=0.0032, Figure 6B). These data demonstrate an increase in immature blood vessels in the lungs of HGF compared to WT littermates. This further suggests, blood vessel formation is continued throughout the animal's lifespan and not completed at earlier development.

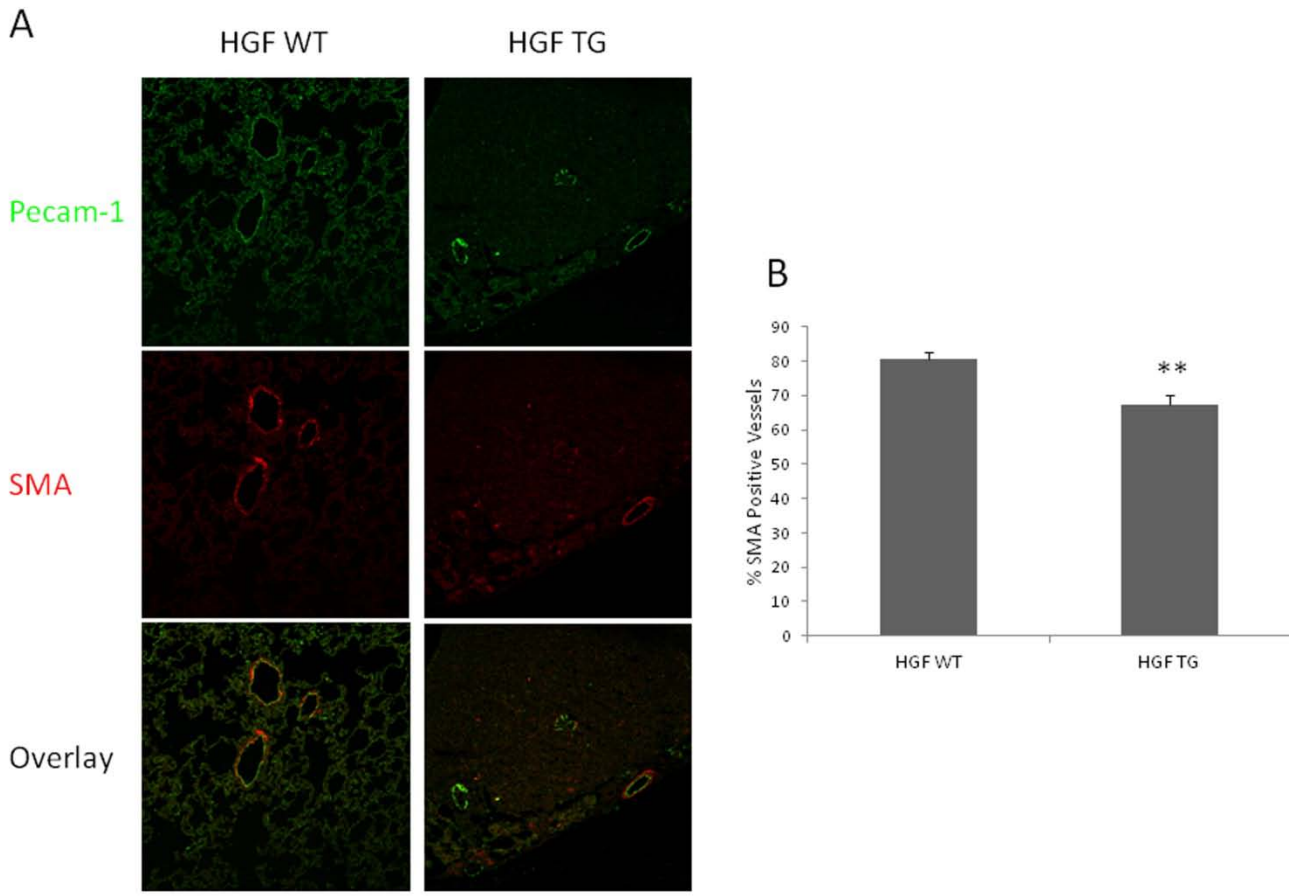

Figure 6. Decreased blood vessel maturity in HGF TG mice compared to WT littermates. A. Representative pictures of dual immunofluorescent staining of the blood vessel marker, PECAM-1 (green), and pericyte marker, SMA (red), from 20 wk old WT and HGF TG mouse lungs. **B.** Vessels stained with PECAM or SMA were counted in 5-10 high-magnification areas per lung of 6 HGF TG and 6 WT mice. Graph depicts the % of SMA positive vessels as determined by dividing average number of SMA vessels by PECAM vessels in HGF TG or WT mice. Asterisk denotes level of significance of HGF TG to similarly aged WT mice (** <0.005)

2.2.4 Over-expression of HGF Increases Lymphatic Vessel Formation.

HGF ligand has been reported as a major inducer of lymphangiogenesis (100). Since lymphatic endothelial cells also express PECAM-1, PECAM staining alone is unable to differentiate between blood and lymph microvessels. In order to determine if HGF-induced blood vessel formation included increased lymphatic vessel formation, lung tissues were stained for lymphatic vessel endothelial hyaluronan receptor-1 (LYVE-1). LYVE-1 is a cell surface receptor specifically expressed on lymphatic endothelial cells (101), and has been used as a marker for lymphangiogenesis in cancer (102, 103). Following LYVE-1 immunohistochemistry (Figure 7A and 7B), vessels were counted in ten high-magnification areas per lung from HGF TG (n=6) and WT (n=6) mice at 20 weeks of age. An excess of lymphatic vessels was observed in HGF TG (9.05 ± 0.2 vessels/1mm2) animals compared to WT (6.32 ± 0.3 vessels/1mm2, P=0.0001) littermates. The ratio of TG:WT lymphatic vessel density at 20 weeks of age was calculated as 1.43 (Figure 7C). This is compared to a ratio of 3.33 for all vessels as determined by PECAM staining at 20 weeks of age (Figure 4E). Thus, vessels arising from the lymphatics accounted for at least part of the total increase in vessel density.

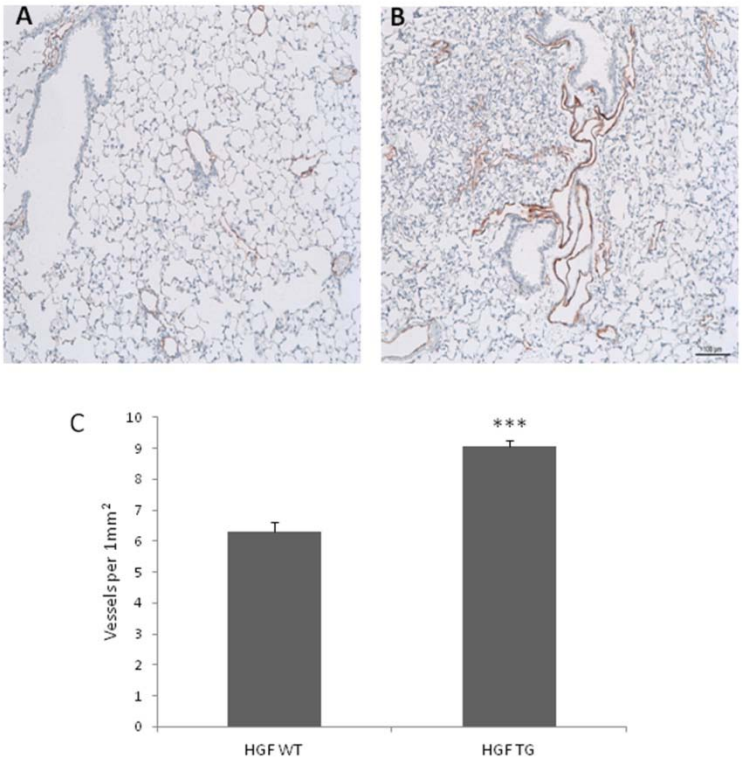

Figure 7. HGF TG mice displayed significantly higher numbers of LYVE-1 positive vessels than similarly aged WT littermates. A,B. Representative pictures from 20wk old WT (A) and HGF TG (B) mouse lungs stained with the lymphatic vessel marker, LYVE-1. **C.** Average number of LYVE-1 positive vessels from 10 high-magnification areas (1mm2) per lung of 6 HGF TG and 6 WT mice. Asterisk denotes level of significance of HGF TG to WT mice (*** <0.001).

2.2.5 Several Angiogenic Factors are Down-regulated in HGF TG Animals Compared to WT littermates.

Cancer Pathway Finder Array

We profiled the expression of 113 genes using the Oligo GEArray Cancer Pathway Finder microarray to determine changes in gene expression associated with the enhanced

vascularization in HGF TG animals. Microarrays were completed using intact whole lungs from HGF TG (n=4) and WT (n=4) non-NNK treated mice (40 weeks of age, Table 2 and Appendix Table 5). The significance threshold was set at a 1.5- or 2.0-fold difference relative to wild-type. Genes are listed in order from most to least changed as determined by the HGF TG to WT ratio, along with the gene symbol, functional grouping, average expression as normalized to *Gapdh*, standard deviation, and P value. Six cancer-related pathways are represented on the array (Cell Cycle Control & DNA Damage Repair, Apoptosis and Cell Senescence, Signal Transduction Molecules and Transcription Factors, Adhesion, Angiogenesis, and Invasion and Metastasis), of which, mRNA expression was preferentially altered in genes involved in angiogenesis (16 of 32 genes were down-regulated). Included in those 16 genes, all members of the VEGF family of angiogenic ligands were significantly reduced (*Vegfd* P=0.0031, *Vegfb* P=0.0043, *Vegfa* P=0.01, *Vegfc* P=0.0361, Table 2). Ratios of TG:WT expression for the four VEGF genes were as follows: *Vegfd* 0.34, *Vegfb* 0.48, *Vegfa* 0.53, *Vegfc* 0.56 (Table 2). The majority of genes on the Cancer Pathway Finder Array were not significantly different in the HGF TG murine lungs compared to WT lung, and none were up-regulated above the 2-fold boundary.

By immunohistochemistry, the c-Met receptor protein appeared somewhat higher in the HGF TG vessels compared to WT mice. The c-Met receptor was included in the microarray, but was not significantly altered in HGF TG animals (Appendix Table 5). The localized change of c-Met receptor within the microvessels may not be reflected in RNA isolated from whole lungs. We also observed that the murine HGF gene was down-regulated (2-fold), although not significantly, in HGF TG lungs compared to WT littermates (Appendix Table 5). This is not unexpected since the transgene is for human HGF. We have previously documented Clara cell-specific over-expression of human HGF in the airways and bronchoalveolar lavage fluid of the

HGF TG animals (86). We would not expect an increase in murine HGF. The decrease in murine HGF may reflect feedback inhibition due to over-expression of the human HGF transgene.

Table 2. Genes with significantly altered expression (>1.5-fold)

		HGF WT		HGF TG			
Symbol	**Functional Gene Grouping**	**Avg**	**STD**	**Avg**	**STD**	**Ratio (TG:WT)**	***p***
10 weeks							
Epas1	Transcription Factor	6.38	0.69	0.76	0.11	0.12	0.0038*
Cdh5	Adhesion Molecule	2.78	1.03	0.35	0.22	0.12	0.0018*
Kdr	Growth Factor Receptor	1.33	0.69	0.17	0.07	0.13	0.0017*
Tbx4	Transcription Factor	0.16	0.74	0.02	0.08	0.13	0.0018*
Eng	Adhesion Molecule	0.60	0.61	0.09	0.10	0.15	0.0039
Tgfb1	Growth Factor	0.28	0.68	0.04	0.10	0.16	0.0001*
Ephb4	Growth Factor Receptor	0.31	0.66	0.05	0.14	0.17	0.0006*
Lama5	Adhesion Molecule	0.18	0.70	0.04	0.12	0.21	0.0119
Mmp2	Invasion & Metastasis/Protease	0.88	0.55	0.22	0.14	0.25	0.0082*
Fgfr3	Growth Factor Receptor	0.58	0.72	0.15	0.13	0.26	0.0067*
Flt1	Growth Factor Receptor	0.40	0.68	0.10	0.18	0.26	0.0009*
Npr1	Growth Factor Receptor	0.12	0.71	0.03	0.14	0.29	0.0029*
Timp2	Invasion & Metastasis/ Angiogenic Inhibitor Protein	1.95	0.67	0.65	0.13	0.33	0.0103
Col4a3	Matrix Protein	0.12	0.97	0.04	0.35	0.35	0.0390
Mapk14	Growth Factor Receptor	0.19	0.65	0.07	0.10	0.38	0.0267
Stab1	Adhesion Molecule	0.10	0.64	0.04	0.20	0.40	0.0063*
Tgfb2	Growth Factor	0.07	0.48	0.03	0.17	0.40	0.0172
Pecam1	Adhesion Molecule	2.85	0.64	1.25	0.15	0.44	0.0035*
Sphk1	Transcription Factor	0.02	0.67	0.01	0.20	0.46	0.0004*
Pdgfa	Growth Factor	0.17	0.68	0.08	0.28	0.46	0.0017*
Mmp9	Invasion & Metastasis/Protease	0.06	0.77	0.03	0.18	0.46	0.0391
Nrp2	Growth Factor Receptor	0.15	0.70	0.07	0.19	0.49	0.0333
Tnfsf12	Adhesion Molecule	0.14	0.60	0.07	0.21	0.54	0.0017*
Plau	Invasion & Metastasis/Protease	0.02	0.71	0.01	0.20	0.63	0.0445
Ptgs1	Signal Transduction Molecule	0.38	0.63	0.25	0.23	0.65	0.0161
Cxcl5	Cytokine	0.00	0.42	0.02	0.23	4.89	0.0252
Il1b	Cytokine	0.22	0.51	1.35	0.34	6.04	0.0343
40 weeks							
Efna2	Signal Transduction Molecule	0.48	0.27	0.09	0.17	0.19	0.0286
Pik3cb	Signal Transduction Molecule	0.57	0.10	0.11	0.05	0.20	0.0285
Cxcl9	Cytokine	0.35	0.19	0.08	0.10	0.23	0.0304
Mmp9	Invasion & Metastasis/Protease	0.25	0.15	0.08	0.01	0.34	0.0250
Figf (Vegfd)	Growth Factor	0.51	0.13	0.18	0.16	0.34	0.0031
Akt1	Signal Transduction Molecule	0.56	0.14	0.20	0.12	0.36	0.0013
angptl4	Angiogenic Inhibitor Protein	0.63	0.21	0.25	0.18	0.40	0.0324
Syk	Signal Transduction Molecule	0.16	0.02	0.07	0.00	0.41	0.0172

Table 2 Continued…

		HGF WT		HGF TG			
Symbol	**Functional Gene Grouping**	**Avg**	**STD**	**Avg**	**STD**	**Ratio (TG:WT)**	***p***
Mmp2	Invasion & Metastasis/Protease	0.29	0.06	0.13	0.05	0.44	0.0004
Pofut1	Signal Transduction Molecule	0.22	0.07	0.10	0.03	0.44	0.0143
Tnfrsf12a	Adhesion Molecule	0.41	0.13	0.18	0.11	0.45	0.0376
Vegfb	Growth Factor	0.69	0.18	0.33	0.15	0.48	0.0043
Efna1	Signal Transduction Molecule	0.42	0.04	0.20	0.17	0.49	0.0459
TNF	Cytokine	0.17	0.04	0.08	0.02	0.49	0.0008
Pik3r1	Signal Transduction Molecule	0.13	0.02	0.06	0.00	0.49	0.0425
Nrp2	Growth Factor Receptor	0.19	0.04	0.10	0.02	0.52	0.0055
Mdk	Growth Factor	0.21	0.05	0.11	0.03	0.53	0.0107
Tgfb3	Growth Factor	0.72	0.15	0.38	0.19	0.53	0.0327
Vegfa	Growth Factor	0.83	0.11	0.45	0.28	0.53	0.0100
Mapk14	Growth Factor Receptor	0.89	0.10	0.48	0.35	0.54	0.0205
Flt1	Growth Factor Receptor	0.89	0.10	0.48	0.35	0.54	0.0205
Csf3	Cytokine	0.32	0.09	0.18	0.07	0.55	0.0422
Vegfc	Growth Factor	0.23	0.08	0.13	0.06	0.56	0.0361
Timp3	Invasion & Metastasis/ Angiogenic Inhibitor Protein	0.94	0.08	0.53	0.28	0.56	0.0065
Grb2	Signal Transduction Molecule	0.11	0.00	0.06	0.00	0.57	0.0046
Anpep	Protease	0.11	0.03	0.07	0.02	0.58	0.0344
Plau	Invasion & Metastasis/Protease	0.11	0.04	0.06	0.01	0.60	0.0457
Col18a1	Angiogenic Inhibitor Protein	0.13	0.03	0.08	0.03	0.62	0.0166
Ptgs2	Signal Transduction Molecule	0.12	0.03	0.07	0.01	0.62	0.0328
Itga2	Adhesion Molecule	0.10	0.00	0.06	0.00	0.64	0.0069
Pdgfa	Growth Factor	0.93	0.08	0.60	0.28	0.65	0.0198
Timp1	Invasion & Metastasis/ Angiogenic Inhibitor Protein	0.11	0.03	0.07	0.01	0.65	0.0169
Eng	Adhesion Molecule	0.09	0.02	0.06	0.01	0.65	0.0357
FGF1	Growth Factor	0.09	0.03	0.06	0.01	0.66	0.0350
IGF1	Growth Factor	0.10	0.02	0.07	0.01	0.67	0.0019

*adjusted p-value <0.05 after application of Benjamini Hochberg correction

Angiogenesis Array

In order to look more closely at which genes may be responsible for the enhanced vascularization, we profiled the expression of 113 genes involved in angiogenesis using commercial angiogenic arrays (Oligo GEArray and Angiogenesis PCR Array) (Figure 8A and 8B). Microarrays were completed on individual whole lungs from HGF TG and WT non-NNK

treated animals of 10 weeks (HGF TG, n=4; WT, n=3) and 40 weeks (HGF TG, n=4; WT, n=4) of age. Twenty-five genes, including VEGF receptor 2 (*Kdr*), neuropilin 1 (*Nrp1*), and transforming growth factor beta 2 (*Tgfb2*) showed a significant 2-fold decrease in expression in HGF TG mice compared to WT littermates at 10 weeks of age. Also at 10 weeks, a significant increase was seen in two pro-angiogenetic genes: chemokine (C-X-C motif) ligand 5 (*Cxcl5*) and *Il1b* (Table 2). At 40 weeks of age, a significant 2-fold decrease was seen for the expression of eight of the same genes as at 10 weeks, such as, *Mmp2, Mmp9,* and neuropilin 2 (*Nrp2)* (Table 2). An additional 21 other genes associated with angiogenesis were also reduced at 40 weeks including angiopoietin-like 4 (*Angptl4*), *Cxcl9*, *Tgfb3*, *Figf* (*Vegfd*), *Vegfa*, *Vegfb*, and *Vegfc* (Table 2). No genes were found to be up-regulated above the 2-fold level at 40 weeks of age. Lung tissue was also analyzed from mice sacrificed at 20 weeks of age. Similar trends were observed in the decreased gene expression comparable to those seen at 10 and 40 weeks, though the changes at 20 weeks were not significant (data not shown). The Benjamini Hochberg method was applied to control for the false-discovery rate, due to the number of mRNA transcripts examined. Comparisons with adjusted p-values that remained significant are indicated with an asterisk within the tables. Since the normalized array data demonstrated reproducible results on both arrays, the chance of spurious result is small. Thus, p-values that did not remain significant after Benjamini Hochberg analysis are not necessarily false.

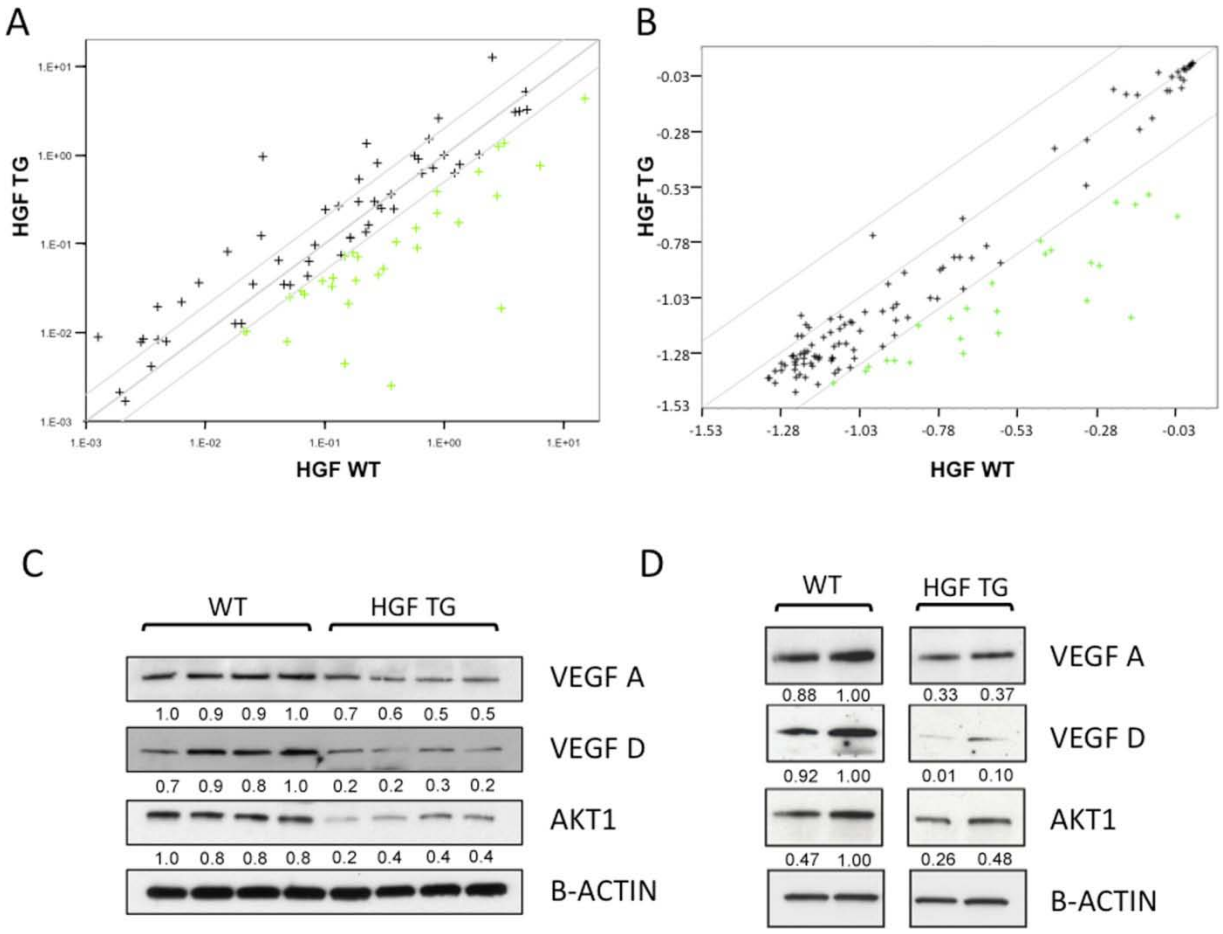

Figure 8. **Whole Lung DNA Microarrays and Western Blot Analysis for genes related to angiogenesis.** Microarray Analysis depicted decreased expression in genes associated with angiogenesis in HGF TG mice compared to WT littermates. **A,B**. Scatter Plot analysis displaying the fold difference in the relative expression levels of genes in the angiogenesis array from 10 wk **(A)** and 40 wk **(B)** HGF TG mice vs. WT. A green (+) represents genes whose fold decrease is greater than the 2-fold boundary. Black asterisks depict unchanged genes. **C,D.** Protein expression of individual whole lungs from 10 wk **(C)** and 40 wk **(D)** old HGF TG and WT mice. Relative densitometry quantitation normalized to β-actin is shown beneath each lane.

A two-dimensional clustergram of the individual lung tissue expression profiles (at 40 weeks) from the angiogenesis array was generated using the normalized expression and an average join type. Individual HGF TG samples were successfully clustered from the WT lungs (Figure 9). VEGF signaling pathway genes shown to be reduced in HGF TG lungs compared to WT by scatterplot were also identified by clustergram and statistical analyses: *Vegfa, Vegfb, Vegfc, Vegfd/Figf, Nrp2, Csf3, Pi3k,* and *Grb2*. The large majority of genes on the angiogenesis array were not significantly different between WT and HGF TG lungs. Those genes with an expression ratio (TG:WT) of at least 0.80 at both 10 and 40 weeks include epidermal growth factor (*Egf*), angiopoietin 1 (*Angpt1*), fibroblast growth factor 2 (*Fgf2*), integrin alpha 5 (*ItgaV*), matrix metallopeptidase 19 (*Mmp19*), and serpin peptidase inhibitor clade F member 1 (*Serpinf1*) (Appendix Table 5).

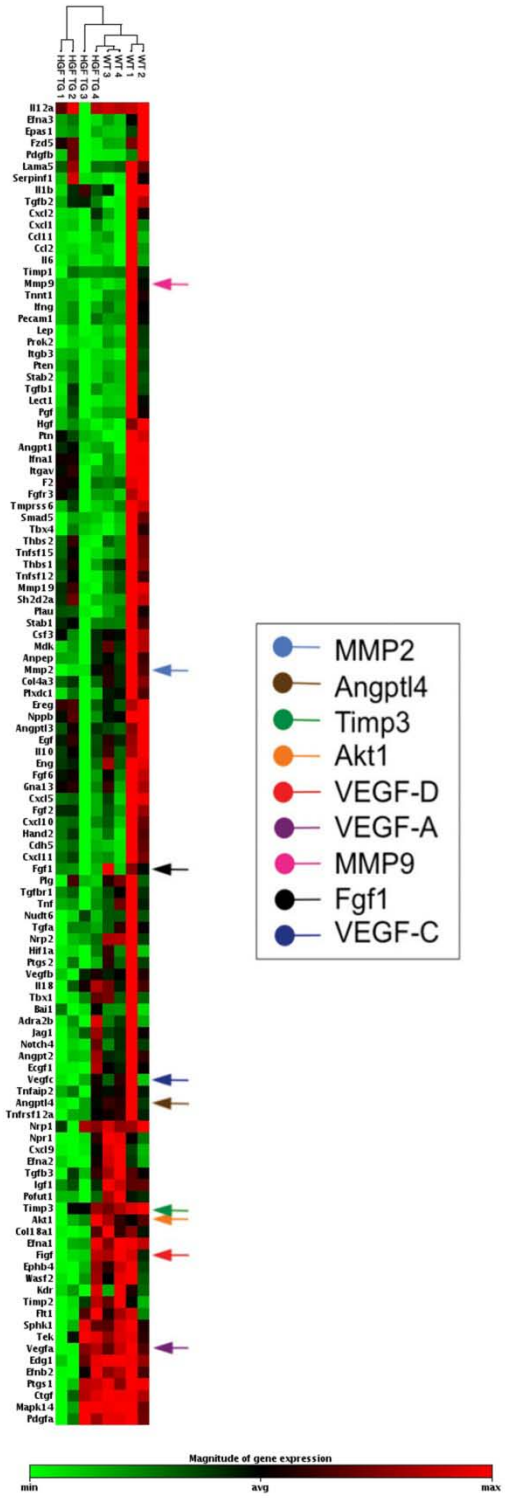

Figure 9. Angiogenesis clustergram. Samples are clustered by gene expression similarity. More similar genes appear lower on the dendrogram and less similar at higher heights. Colored arrows point to the genes of interest indicated by the legend.

Western Analysis

Western blot analysis verified several genes whose expression was decreased on the microarrays. Protein was extracted from whole lung tissue from the same mice utilized for the microarray analysis. The VEGFA, VEGFD, and AKT1 genes, identified as down-regulated in microarray analysis at 10 weeks (Figure 8A) and 40 weeks (Figure 8B), demonstrated reduced protein expression in HGF TG mice compared to WT littermates at both 10 (Figure 8C) and 40 (Figure 8D) weeks of age. The following percent decrease in protein expression was determined after normalizing to ß-actin: VEGFA (40.2% 10 weeks, 62.4% 40 weeks), VEGFD (73.3% 10 weeks, 94.4% 40 weeks), and AKT1 (60.2% 10 weeks, 49.7% 40 weeks). Verification of microarray results by protein analysis at multiple time points further suggests that genes found statistically significant before exclusion by the Benjamini Hochberg method are not necessarily false.

2.2.6 VEGFR2 Inhibition does not Block Increased Vascularization in HGF TG animals.

Expression data demonstrated VEGF mRNA and protein was significantly reduced in HGF TG mice compared to WT littermates at 40 weeks of age and down-regulated or found at comparable levels at 10 weeks of age. Thus, the increased vascularization seen in HGF transgenic animals is expected to be largely VEGF-independent. To further confirm that VEGF is not required for enhanced blood vessel formation in vivo, WT and HGF TG mice were treated with vandetanib. Vandetanib is a tyrosine kinase inhibitor of VEGFR2/3 (104). VEGFR3 is the major receptor responsible for endothelial cell proliferation in response to VEGF stimulation (104). To a lesser extent, Vandetanib also inhibits EGFR (104). To account for this, mice were also treated with gefitinib, a selective EGFR inhibitor. Any differences observed in vascularization after

vandetanib treatment, which were not observed with gefitinib treatment, could be attributed to VEGF inhibition exclusively.

HGF TG (n=3) and WT (n=3) littermates were treated with vehicle control (1% Tween-80/0.9% saline), gefitinib (75mg/kg), or vandetanib (25mg/kg) for five weeks, beginning at five weeks of age. Whole lungs were collected at 10 weeks of age and sectioned for PECAM immunohistochemistry. A significant increase of blood vessel density was seen in HGF TG animals compared to WT littermates regardless of treatment (Table 3). Vandetanib and gefitinib treatments had no effect on normal microvessel density in WT mice (5.52 ± 0.33 microvessels/area, 6.52 ± 0.36 microvessels/area respectively) as compared to control WT littermates (4.63 ± 0.28 microvessels/area (n.s., vandetanib or gefitinib vs. control)). As expected, blood vessel density was significantly increased in control HGF TG mice at 10 weeks (8.00 ± 0.48 microvessels/area) compared to control WT littermates (4.63 ± 0.28 microvessels/area, $P<0.001$). Vandetanib treatment did not modify microvessel density in HGF TG mice (8.79 ± 0.59 microvessels/area) compared to control HGF TG animals (8.00 ± 0.48 microvessels/area, $P > 0.05$). Blood vessel density in HGF TG lungs from vandetanib treated mice remained significantly increased from WT mice either with or without vandetanib treatment ($P < 0.001$ for both comparisons). Gefitinib treatment slightly increased microvessel density in HGF TG mice (10 ± 0.42, $P=0.049$), compared to control transgenic animals. Thus, inhibiting EGFR in the presence of HGF over-expression slightly promotes new blood vessel formation. Gefitinib has been reported to inhibit recruitment of pericytes to blood vessels (105). By maintaining blood vessels in an immature state, endothelial cell growth and migration could be continued in the presence of elevated HGF. These data further establish that VEGF pathways do not play a major role in microvessel formation in the lungs when HGF/c-Met activation is high.

Table 3. Blood vessels per area comparison.

Treatment	**WT**	**HGF TG**
Vehicle	4.6 ± 0.3	8.0 ± 0.5
Gefitinib	6.5 ± 0.4	10 ± 0.4
Vandetanib	5.5 ± 0.3	8.8 ± 0.6
Comparisons	**Mean Difference**	***p***
Vehicle WT vs Vehicle TG	-3.37	< 0.001
Vehicle WT vs Gefitinib WT	-1.89	> 0.05
Vehicle WT vs Vandetanib WT	-0.89	> 0.05
Vehicle WT vs Vandetanib TG	-4.15	< 0.001
Vehicle TG vs Gefitinib TG	-2.00	< 0.05
Vehicle TG vs Vandetanib TG	-0.78	> 0.05
Gefitinib WT vs Gefitinib TG	-3.48	< 0.001
Vandetanib WT vs Vandetanib TG	-3.26	< 0.001

2.2.7 Lung Tumors from Transgenic Mice Demonstrate a Similar Decrease in Angiogenic Genes as Whole Lung Analysis, with Increased Expression of Inflammatory Related Genes.

All of the previously discussed work was carried out on whole lungs of HGF TG and WT animals. To determine if lung tumors demonstrate similar patterns of down-regulated angiogenic genes, HGF TG and WT mice were injected with NNK and individual tumors were collected. Microarray analysis on tumors from HGF TG mice (n=4) was compared to lung tumors from WT mice (n=4). Representative arrays from HGF TG and WT are shown in Figure 10. Many of the same genes, which were found to be down-regulated in HGF TG whole lung, showed a significant 2-fold or greater decrease in expression in HGF TG tumors compared to WT tumors. The down-regulated genes included *Mmp2*, *Akt1*, *Timp3*, and the *Vegfa*, *Vegfb*, *Vegfc*, and *Vegfd/Figf* (Figure 10B). The majority of genes on the both the Cancer Pathway Finder and

Angiogenesis Arrays were shown to have comparable expression between HGF TG and WT individual tumors (Table 4). Three genes had a high TG:WT ratio in whole lung expression; *Angptl1*, *Fgf2*, and *ItgaV*. These three genes also showed a ratio of 1.0 or higher in HGF TG tumors compared to WT tumors (Table 4). Five genes were found to be significantly up-regulated in the HGF TG tumors compared to WT tumors. All five belong to the chemokine (C-X-C motif) ligand family: *Cxcl1*, *Cxcl2*, *Cxcl10*, *Cxcl11*, and *Cxcl9* (Table 4). *Cxcl1* and *Cxcl2* are murine homologs of IL8, a potent angiogenic chemokine.

Table 4. Expression of genes in HGF TG lung tumors.

	WT Tumor		**TG Tumor**			
Symbol	**Avg**	**STD**	**Avg**	**STD**	**Ratio (TG:WT)**	***p***
Angiogenesis Array						
Cxcl1	0.16	0.01	0.41	0.01	2.55	0.002*
Cxcl11	0.15	0.01	0.32	0.01	2.21	0.002*
Cxcl10	0.25	0.02	0.45	0.01	1.79	0.006
Cxcl2	0.17	0.02	0.30	0.00	1.75	0.010
Cxcl9	0.43	0.04	0.73	0.00	1.71	0.008
Ifng	0.18	0.01	0.26	0.00	1.46	0.084
Il1b	0.63	0.06	0.78	0.01	1.24	0.677
Tnfaip2	0.27	0.04	0.32	0.02	1.20	0.994
Cxcl5	0.11	0.00	0.11	0.00	1.01	0.405
Cancer Array						
Fgfr2	0.12	0.01	0.15	0.04	1.19	0.497
Mmp9	0.15	0.01	0.18	0.08	1.17	0.690
Atm	0.11	0.01	0.12	0.01	1.17	0.142
Cdh1	0.41	0.19	0.46	0.13	1.14	0.756
Birc5	0.09	0.00	0.10	0.02	1.13	0.538
Cdc25a	0.28	0.00	0.31	0.01	1.11	0.072
Bai1	0.08	0.01	0.09	0.02	1.09	0.690
Cflar	0.13	0.01	0.14	0.03	1.08	0.686
Brca1	0.11	0.00	0.12	0.02	1.06	0.600
Cdk2	0.10	0.01	0.11	0.01	1.05	0.714
Bak1	0.17	0.01	0.18	0.01	1.04	0.541
Ifna1	0.14	0.01	0.14	0.01	1.03	0.561
Ccne1	0.17	0.01	0.17	0.02	1.03	0.826
E2f1	0.09	0.01	0.10	0.02	1.03	0.887
Angpt1	0.10	0.01	0.11	0.02	1.02	0.843

Table 4 Continued…

	WT Tumor		TG Tumor			
Symbol	**Avg**	**STD**	**Avg**	**STD**	**Ratio (TG:WT)**	***p***
Cd44	0.52	0.12	0.53	0.09	1.02	0.919
Brca2	0.10	0.00	0.10	0.02	1.02	0.857
Fgf2	0.09	0.00	0.09	0.02	1.02	0.914
Icam1	0.75	0.06	0.76	0.10	1.01	0.902
Tgfb1	0.80	0.08	0.81	0.05	1.01	0.882
Cdk4	0.93	0.03	0.94	0.01	1.01	0.775
ItgaV	0.09	0.01	0.09	0.02	1.00	0.996
Ifnb1	0.09	0.01	0.09	0.02	1.00	0.997
Tnf	0.14	0.00	0.14	0.05	1.00	0.998

*adjusted p-value <0.05 after application of Benjamini Hochberg correction

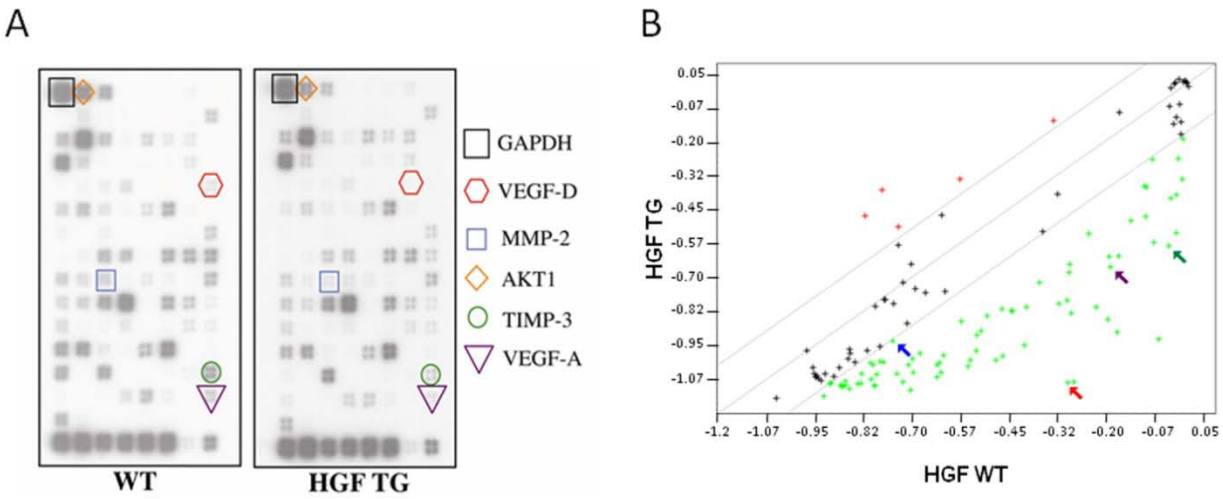

Figure 10. **Tumor DNA Microarray Analysis for genes associated with angiogenesis.** Similar patterns of down-regulated gene expression were seen in NNK induced tumors from HGF TG mice compared to WT littermates. **A.** Representative hybridization blots from HGF TG and WT mice. Colored boxes highlight specific significantly down-regulated genes. **B.** Scatter plot displaying the fold difference in the relative expression levels of genes of isolated NNK induced lung tumors from HGF TG and WT mice (40 weeks old). A green (+) represents genes whose fold decrease is greater than the 2-fold boundary. Black (+) depicts unchanged genes. Red (+) represents genes whose fold increase is greater than the 2-fold boundary. Colored arrows point to corresponding genes as indicated on microarray blots.

2.3 CONCLUSIONS AND DISCUSSION

Although the angiogenesis process in lung cancer has been considered to be largely dependent on the VEGF pathway (88, 89), our results support the hypothesis that different signaling pathways can drive vessel formation. Lungs, in the presence of high HGF expression, demonstrated vigorous and constant increasing vascularization compared to wild-type littermates. These vessels uniformly expressed c-Met protein, and thus are able to respond to increased HGF ligand directly. We observed that microvessels in HGF over-expressing mice were significantly less mature than their WT counterparts. These data support the idea that HGF ligand continually enhances blood vessel formation over time. In addition to blood vessel enhancement, HGF over-expression was shown to induce lymphatic vessel growth. Lymphatic vessels, which are known to be stimulated by HGF (100), accounted for one-third of the total enhanced vessel density in this study.

Gene expression analysis produced mRNA profiles for HGF TG and WT animals. The lungs of HGF TG mice displayed significantly reduced gene expression in pro-angiogenic molecules such as the VEGF family and genes associated with the VEGF pathway such as *Nrp2*. This pattern of decreased expression was seen in HGF TG mice compared to WT littermates 10, 20, and 40 weeks of age. Western blot analysis confirmed that VEGF genes maintained reduced protein levels in 10 and 40 week HGF over-expressing mice compared to WT. Furthermore, vandetanib treatment of HGF TG mice at an early age failed to inhibit the enhanced vascularization documented in HGF TG animals. This further suggests HGF acts independently of VEGF pathway to stimulate vascularization. There was no significant change in the genes related to apoptosis, proliferation, or oncogenic pathways contained in these arrays. Thus, in the

absence of injury, such as a carcinogenic treatment, HGF over-expression in the lungs of transgenic animals produces angiogenic effects over oncogenic signals; similar to the role HGF plays in wound healing. Previous observation revealed heterozygous HGF TG mice do not develop lung tumors spontaneously (86). Lung adenoma and adenocarcinoma formation remain dependent on carcinogen exposure.

It is possible that HGF-induced vascularization occurs through transcription of genes not represented on the gene arrays utilized, thus accounting for the lack of up-regulated gene expression seen in this study. Alternatively, much of the increased in blood vessels could be through direct effects of the transgenic HGF protein on endothelial cells that do not require increased synthesis of the mRNAs examined. For example, HGF, via the c-Met receptor, could directly activate integrins expressed on endothelial cells to promote their movement and proliferation (92). Release of pre-synthesized angiogenic proteins from infiltrating macrophages and neutrophils, such a ELR+ CXC chemokines, also would not require new mRNA synthesis of angiogenic factors and could act directly on endothelial cell receptors (29). It is also possible that since the blood vessels were not microdissected for RNA extraction, we were only able to observe gene expression changes occurring in whole lung, and could not measure local changes in mRNAs needed for increased vascularization in response to HGF.

Tumor gene expression data mimicked profiles seen in whole lung analysis. However, a significant increase in five chemokine (C-X-C motif) ligand family members was seen in HGF TG lung tumors compared to WT tumors. These included both pro-angiogenic ELR+ and angiostatic ELR- CXC chemokines. There was no significant change in mRNA expression for whole lung samples of the functional homologues of IL-8 (*Cxcl2* and *Cxcl1*) or IL-1ß at 40 weeks. A significant up-regulation of *Cxcl5*, another pro-angiogenic CXC chemokine, and IL-1ß

was seen in HGF TG mice at 10 weeks of age. IL-8 and IL-1ß have been identified as potential mediators for HGF-induced angiogenesis in HNSCC (33, 106), and nasopharyngeal cancer (NPC) (91). Co-expression of HGF and IL-8 in NPC has been shown to be associated with increased microvessel density and poor prognosis (91). HGF has also been reported to induce IL-8 expression in lung adenocarcinoma cells (90). The increased expression of *Cxcl1*, *Cxcl2*, and IL-1ß in whole lung samples (10 weeks) and HGF TG tumors indicates these chemokines play a role in HGF-mediated normal vascularization as well as tumorigenesis in the lung. Angiostatic ELR- CXC chemokines were also up-regulated in HGF TG tumors, but to a lesser extent than pro-angiogenic ELR+ factors. This increase may be due to an attempt to balance the rise in pro-angiogenic factors.

There was no significant down regulation of genes such as caspase-9 or *Bax* that would imply decreased apoptosis is occurring in untreated HGF TG lungs. Additionally, no other genes related to proliferation or oncogenesis contained on these microarrays were found to be elevated. These results further suggest that in the absence of injury, angiogenic effects of HGF over-expression predominate over oncogenic signals.

Overall these results suggest the main effect of HGF over-expression in the transgenic mice is enhanced vascularization accompanied by reduced VEGF pathway genes in lung tissues. Decreases in VEGF may be a feedback mechanism in response to heightened microvessel density as stimulated by HGF. Down-regulation of VEGF through high HGF expression could explain resistance to anti-VEGF therapies currently being tested in several types of cancer including NSCLC (17, 19). Tumor inhibition by VEGF inhibitor in mice was not as effective in HNSCC cells that showed relative VEGF down-regulation (106). Also, elevated HGF levels were associated with colorectal cancer progression in patients being treated with bevacizumab

(21). Similarly, c-Met signaling plays a role in sunitinib resistance (19). Resistant tumors contained higher HGF concentrations and c-Met expression compared to sensitive tumors. In this study, dual treatment with sunitinib and a c-Met inhibitor significantly inhibited tumor growth compared to sunitinib alone and largely targeted the vasculature in resistant tumors (19).

Our HGF TG mouse model could be used to further examine agents that selectively inhibit angiogenesis via VEGF-independent pathways, and lead to new insights into the pathogenesis of NSCLC. It would also be useful in the examination of new anti-angiogenic approaches, either through HGF/c-Met inhibition, or combination with VEGF inhibitors. The complete inhibition of angiogenesis in lung cancer may require novel compounds that target angiogenesis through multiple pathways.

3.0 DELAYED C-MET SIGNALING INDUCES P-STAT3

3.1 INTRODUCTION

Recent efforts in the battle against lung cancer have focused on targeting specific lung cancer-related growth factor pathways such as the VEGFR and EGFR signaling pathways. Unfortunately there has been a lack of clinical efficacy reported for these inhibitors (51). Compensatory signaling from the HGF/c-Met pathway has been reported to play a role in the resistance to both VEGFR and EGFR inhibition (51). Acquired resistance to EGFR tyrosine kinase inhibitors (TKI) has been linked to c-Met in EGFR mutant lung cancer cells (51). Crosstalk between similar pathways has been described in several studies as one method for resistance to receptor blockade (75, 79). In these cases, as the tumor progresses, signaling shifts from one RTK to another. EGFR family members are co-expressed with c-Met receptors in many human tumors including NSCLC (78). Both pathways initiate similar downstream effector molecules such as PI3K/AKT, K-Ras/MAPK, and STAT. These pathways play critical roles in tumor growth and metastasis.

Lateral signaling between c-Met and EGFR has been implicated to be required for cell migration, invasion, and survival (75, 80). Our laboratory has previously determined that crosstalk from the EGFR pathway results in a delayed and prolonged activation of c-Met signaling in NSCLC (80). Delayed c-Met activation by EGF was shown to mediate EGFR-

induced invasion, motility, and proliferation. Early evidence suggests EGF induced delayed c-Met signaling mediates alternative signaling cascades than those seen by HGF stimulation. We hypothesized that delayed c-Met activation amplifies EGF-induced invasion and migration through prolonged activation of mediators such as STAT3. Identification of mediators downstream of EGFR induced delayed c-Met signaling could make for ideal candidates for individual or combinational therapeutic targeting, in order to circumvent survival signaling to compensatory pathways in NSCLC. STAT3 was thought to be a likely candidate because it is known to mediate invasion in other systems. To address the hypothesis, the time course of STAT3 activation following EGFR stimulation and the mechanism of delayed STAT3 activation were studied.

3.2 RESULTS

3.2.1 EGFR Ligands Induce Biphasic Activation of STAT3 in NSCLC cells.

EGFR ligands have been previously shown to induce delayed and prolonged phosphorylation of c-Met receptors in NSCLC cells (80). In that study, c-Met phosphorylation first appeared at 8 hours and was sustained for 48 hours after treatment with EGF. STAT3 belongs to the group of STAT family transcription factors. When activated downstream of growth factors such as EGF and HGF, STAT family transcription factors up-regulate genes related to invasion and cell growth (107, 108). In order to determine whether STAT3 plays a role in delayed c-Met signaling, 201T cells were treated with EGF or HGF for 0-24 hours. Protein lysates from several time points were collected and analyzed for STAT3 phosphorylation (Figure 11). Both HGF and EGF

stimulation induced phospho-STAT3 within 5 minutes. However, while HGF stimulated STAT3 phosphorylation was quickly terminated (Figure 11A), EGF activated STAT3 in a biphasic manner (Figure 11B). While initial activation of STAT3 was reduced to near baseline levels 2 hours post-treatment, a second wave of activation was initiated 8 hours post-treatment and was sustained for 24 hours. This biphasic regulation of STAT3 phosphorylation by EGF mimics the pattern of c-Met and c-Src phosphorylation previously noted by our laboratory (80).

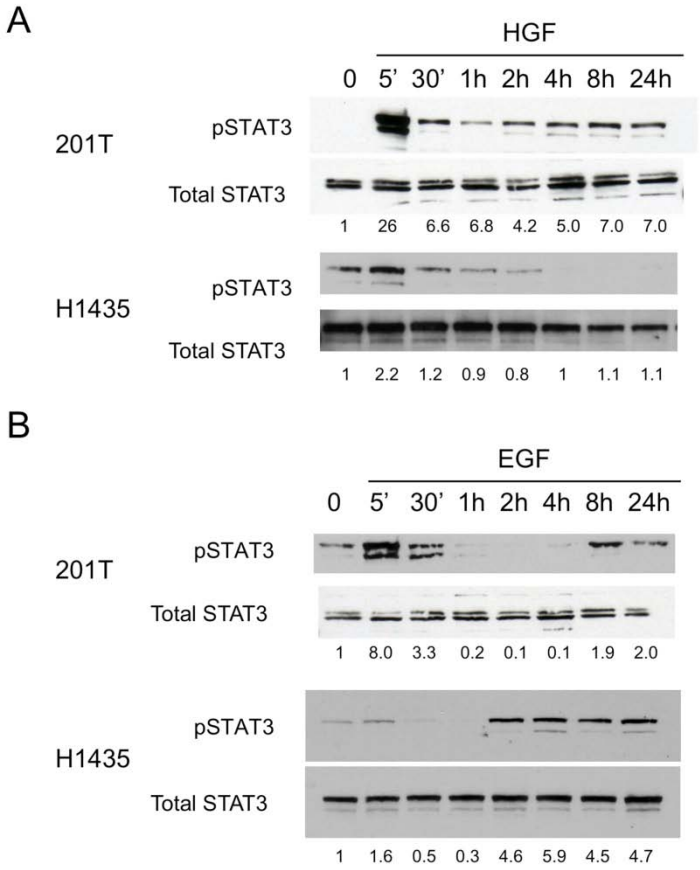

Figure 11. **EGFR ligands induce biphasic activation of STAT3.** 201T and H1435 cells were serum deprived 48 hours prior to treatment with (**A**) HGF (10ng/mL) or (**B**) EGF (10nM) for the indicated time points. Cell lysates were analyzed for STAT3 phosphorylation and expression.

Activated STAT proteins must dimerize and translocate to the nucleus in order to bind to specific target gene promoters (107, 108). To confirm that the delayed phosphorylation of STAT3 by EGF resulted in biologically active STAT3, nuclear lysates from time course experiments with 201T cells were collected and analyzed for STAT3 phosphorylation. A pattern of biphasic phosphorylation was seen in the nuclear extracts similar to that seen with whole cell lysates (Figure 12).

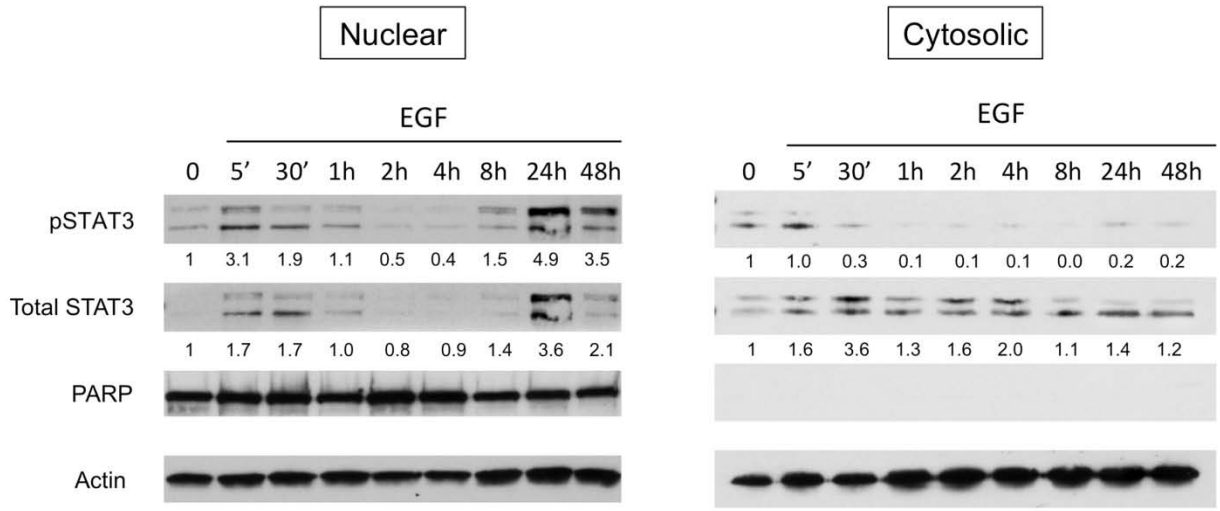

Figure 12. **EGFR simulated STAT3 transnuclear location mimics biphasic pattern.** 201T cells were treated with EGF (10nM) for various time points after 48 hours serum starvation. Cell lysates were fractionated into nuclear and cytosolic portions and analyzed for phospho- and total STAT3 levels. PARP detection validated nuclear and cytoplasmic separation. Actin confirmed equal loading of gels.

3.2.2 Delayed Activation of STAT3 is downstream of c-MET.

The pattern of STAT3 phosphorylation suggests an association between prolonged STAT3 activation and delayed c-Met signaling following EGF stimulation. C-Met may be utilizing STAT3 to amplify and prolong signaling from EGFR. To further investigate whether c-Met activation was required for prolonged STAT3 phosphorylation, 201T cells were pre-treated with the specific c-Met inhibitor, PHA665752 (1 μM), for 2 hours followed by time course analysis of EGF stimulation. Inhibition of c-Met had no effect on the rapid EGF-induction of STAT3 phosphorylation, suggesting early activation by EGFR signaling cascade is not affected by c-Met (Figure 14). However, inhibition of c-Met abolished the bisphasic pattern of STAT3 activation, reducing delayed phospho-STAT3 levels to baseline (Figure 13). This suggests that c-Met is required to prolong EGFR signaling through the STAT3 protein.

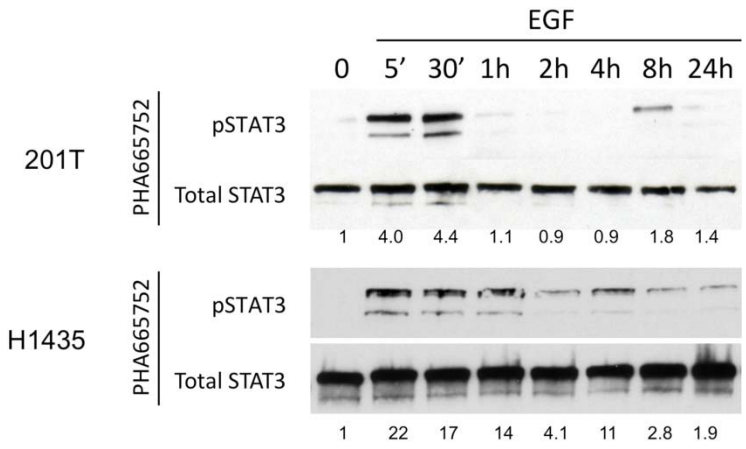

Figure 13. **C-Met is required for delayed phosphorylation of STAT3.** 201T and H1435 cells were serum deprived for 48 hours. Cells were pretreated with PHA665752 (1μM), a Met inhibitor, for 2 hours followed by stimulation with EGF (10nM) for the indicated time points. Cell lysates were analyzed for total and phospho-STAT3 expression.

3.2.3 C-Src does not Mediate delayed c-Met Activation of STAT3.

The biphasic regulation of STAT3 phosphorylation by EGF mimicked the pattern of c-Src phosphorylation previously noted by our laboratory (80). STAT3 activation via EGFR ligand stimulation has been well characterized and is believed to occur through a variety of mechanisms (108, 109), including direct interaction with c-Src. Sustained signaling from c-Met to c-Src could allow STAT3 to be continually phosphorylated, dimerized, and translocated to the nucleus for transcription up-regulation. In order to test if c-Src played a mediator role between c-Met and STAT3 activation, 201T cells were treated with EGF for 30 minutes prior to addition of a SFK inhibitor, PP2 (500nm). Lysates were collected 2-48 hours post-EGF stimulation. Since c-Src has been shown to be integral upstream of delayed c-Met activation (80), PP2 was added early enough to inhibit the second wave of Src activation, while still allowing for induction of phospho-Met. Inhibition of c-Src by PP2 at delayed time points had no effect on phospho-STAT3 levels (Figure 14). PP2 treatment was effective as shown by successful inhibition of p-Src (Figure 14). This suggests c-Src, while activated at delayed time points, does not mediate c-Met signaling to STAT3 activation and translocation.

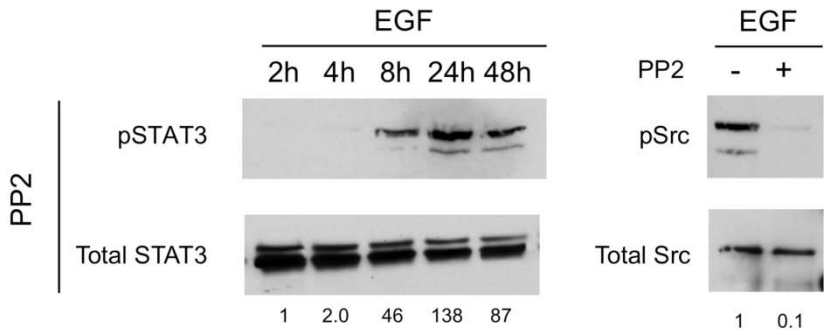

Figure 14. **C-Src does not mediate EGFR-induced delayed activation of STAT3.** 201T cells were serum starved 48 hours prior to stimulation with EGF (10nM). The c-Src inhibitor, PP2 (1μM), was added one hour post stimulation with EGF. Lysates were collected and analyzed for phospho- and total STAT3, or phospho- and total c-Src.

3.2.4 C-Met Directly Interacts with STAT3.

The involvement of c-Src as a mediator between c-Met and STAT3 activation was ruled out by the inability of PP2 to block delayed phospho-STAT3. While other effectors could potentially mediate c-Met signaling to STAT3 activation, direct association of STAT3 through its Src homology-2 (SH2) domain with c-Met can also result in its phosphorylation (110). Therefore, we examined whether c-Met interacts with STAT3 after exogenous EGF addition. Following EGF stimulation for 2-48 hours, co-immunoprecipitation of 201T lysates demonstrated that STAT3 could associate with c-Met at delayed time points (Figure 15). This suggests that STAT3 activation 8-48 hours after EGF stimulation is due to direct activation by c-Met.

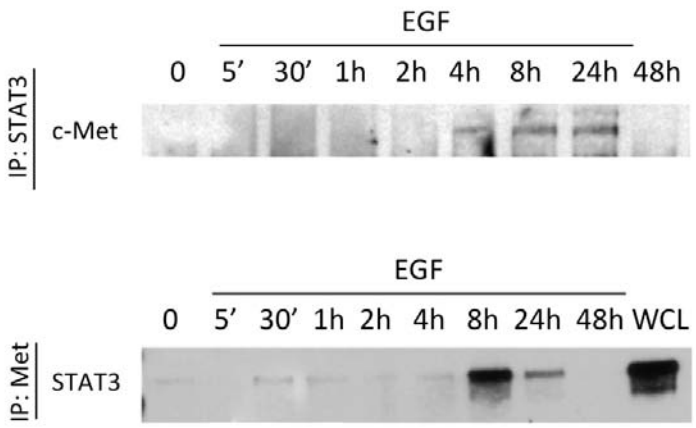

Figure 15. **STAT3 associates with c-Met at delayed time points.** 201T cells were serum starved 48 hours prior to time course stimulation with EGF (10nM). Lysates (400μg) were immunoprecipitated with total STAT3 or c-Met and blotted for c-Met or STAT3 respectively.

3.3 CONCLUSIONS AND FUTURE DIRECTION

While EGFR has been the focus of targeted therapeutics in NSCLC, resistance is common and lessens clinical value. Acquired resistance to EGFR has been linked to compensatory signaling from the HGF/c-Met pathway (51). Evidence of lateral signaling between EGFR and c-Met has been determined to occur in several cancer types (75, 79). Our laboratory recently discovered crosstalk from the EGFR pathway results in prolonged c-Met activation in NSCLC (80). Delayed c-Met signaling following EGF-stimulation appears to utilize separate mediators involved in tumorigenesis compared to transient activation. To date, delayed c-Met signaling has been shown to be independent of MAPK and AKT1 activation (80). The only molecule whose activation has

been identified to require EGFR to c-Met lateral crosstalk is STAT3. STAT3 is known to act downstream of HGF stimulated c-Met to control tublogenesis, wound healing, anchorage-independent growth, and invasion (107). It also plays an important function in the invasive growth response to EGFR ligand stimulation. We previously determined that delayed c-Met activation was required to obtain maximal EGFR-induced invasion, motility, and proliferation in NSCLC cells (80). It is possible that EGFR utilizes c-Met to amplify downstream signaling cascades that are initially activated early on.

The results from this study support the hypothesis that prolonged activation of STAT3, which is dependent on direct interaction with c-Met, may be a key mechanism responsible to produce maximal cell movement and invasion after EGFR activation (Figure 16).

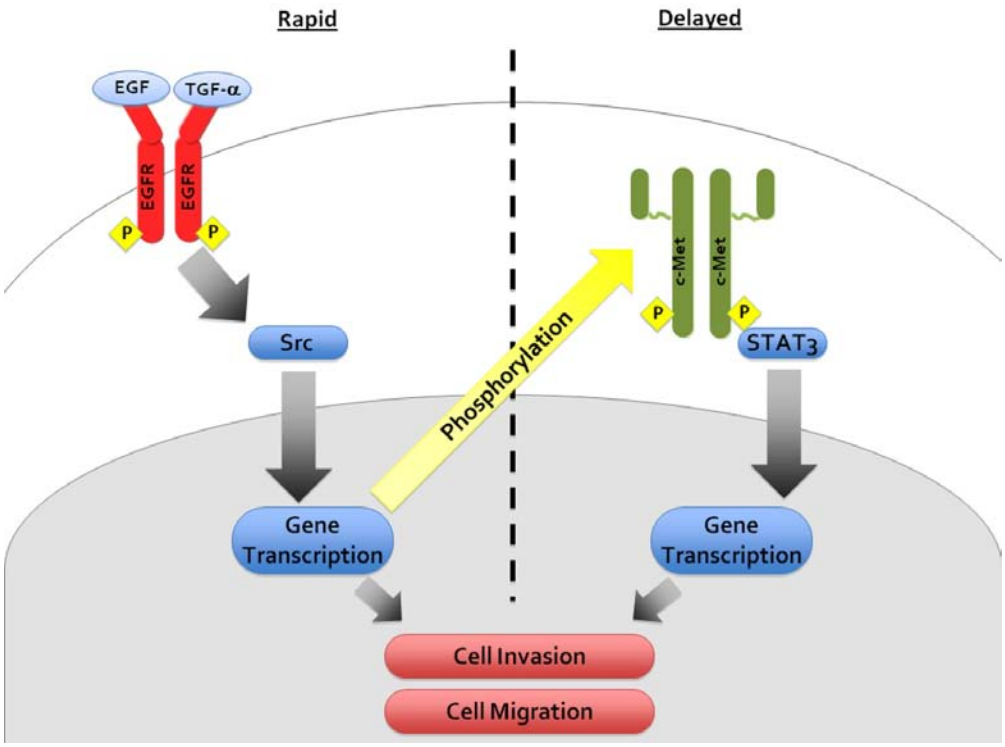

Figure 16. Model of EGFR-induced c-Met activation of STAT3 in NSCLC.

We demonstrated that STAT3 phosphorylation occurs downstream of delayed c-Met activation in NSCLC cell lines. A biphasic pattern of STAT3 activation appears when NSCLC cells are stimulated with EGFR ligands. Transient activation by EGFR at early time points is unaffected by c-Met inhibition. Yet, when delayed c-Met signaling was blocked by PHA665752 phosphorylation of STAT3 was also diminished. One mechanism of growth factor stimulation to STAT3 phosphorylation is through direct c-Src activation (100). However, our initial hypothesis that c-Src mediates c-Met to STAT3 activation has been disproved. Treatment with the c-Src inhibitor, PP2, was unable to hinder activation of STAT3 at later time points (8-48 hours after EGF stimulation). C-Met has is capable of interacting with and activating STAT3 through its SH2 domain (110). Co-immunprecipitation experiments revealed associations between STAT3 and c-Met 8-24 hours post-EGFR ligand stimulation. This suggests activated c-Met is directly acting upon STAT3 to induce phosphorylation and nuclear accumulation. The biological activity of STAT3 as a transcription factor requires cytoplasmic-nuclear translocation of STAT proteins (107). Free cytosolic diffusion from the plasma membrane to the nucleus is a favored model for this translocation. However, there has been more evidence of RTKs, including c-Met, signaling from endosomal compartments and not at the plasma membrane. In fact, when stimulated by HGF, STAT3 phosphorylation and nuclear translocation has been shown to require nuclear-proximal activated c-Met in HeLa cells (107). In that study, sustained phosphorylation of STAT3 was dependent on c-Met being delivered to a perinuclear endosomal compartment. It is possible that the delayed c-Met mode of signaling occurs through intracellular relocalization of c-Met molecules. These subcellular populations may then interact with different effector molecules as seen in the canonical pathway.

These downstream effectors of the delayed c-Met signaling cascade following EGF-stimulation have yet to be discovered. In order to determine which mediators are modulated in response to delayed c-Met activation, whole genome microarray analysis will be completed. 201T cells have been transiently transfected with siRNA for non-targeting (NT) or c-Met. Transfected cells were stimulated with EGF for 0, 24, or 48 hours, or HGF for 5 minutes. RNA and protein was collected to confirm c-Met was knocked down through analysis by RT-PCR or Western blot (Figure 16). RNA will be subjected to whole genome microarray analysis on Illumina Bead Chips and analyzed using BRB array software. The results will be confirmed in NSCLC cell lines and used as a starting point for the identification of novel targets for inhibition of EGFR and c-Met signaling cascades. We are particularly interested in observing differences in genes that are transcriptionally activated by STAT3 (MMP-2, MMP-9, integrin β6).

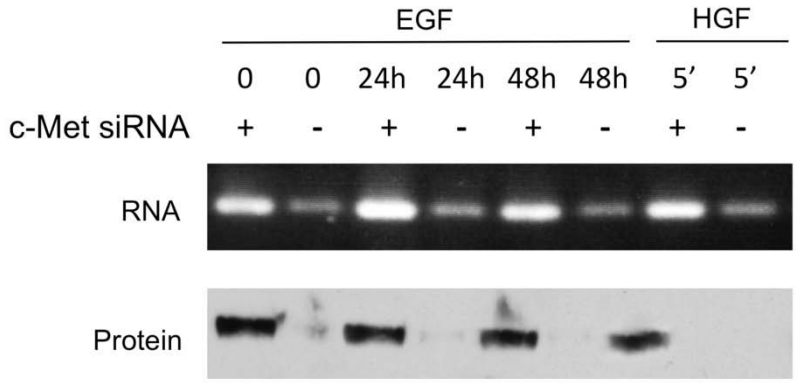

Figure 17. **C-Met siRNA successfully knocks down c-Met RNA and protein levels.** 201T cells were treated with either non-targeting siRNA (NT) or c-Met siRNA for 8 hours. Cells were then serum starved 24 hours prior to treatment with EGF (0, 24, 48 hours) or HGF (0, 5 minutes). RT-PCR for c-Met was performed on extracted RNA. Protein lysates were also analyzed for total c-Met.

4.0 DISCUSSION

This project was focused on aspects of the HGF/c-Met signaling pathway that are relevant to lung cancer. Growth factor stimulation of angiogenic and invasive phenotypes is well known to contribute to the promotion and progression of malignancies, including NSCLC (11, 12). To this extent VEGF and EGFR signaling pathways have been predominantly studied in the past. However, several clinical trials have shown resistance to targeted VEGFR and EGFR therapies. Activating mutations of downstream effector molecules and compensatory signaling from overlapping growth factor pathways are two of the main contributors for resistance (12). The HGF/c-Met signaling pathway has been shown to confer resistance to both VEGFR and EGFR therapeutics in NSCLC (21, 51, 84, 98). This coupled with the strong correlation between HGF and/or c-Met expression with poor patient survival (70-72), supports the hypothesis that HGF/c-Met pathway plays an important role in the pathogenesis of human cancers and is a potential target for therapeutic intervention.

The first aspect of c-Met signaling in this study was focused on the ability of over-expressed HGF to promote angiogenesis in normal whole lungs and lung tumors. We observed an increase in microvessel density in HGF TG animals compare to WT littermates that increased with age. Further characterizing blood vessel formation in these mice, we validated that endothelial cells in the HGF TG and WT mice both express the c-Met receptor. Thus, suggesting HGF may directly stimulate these cells to promote vessel formation. A higher percentage of

immature vessels (as determined by the absence of SMA) was seen in HGF TG mice compared to WT littermates at an intermediary age of 20 weeks. This confirms HGF over-expression continually stimulates blood vessel formation throughout the animal's life. A higher percentage of lymphatic vessels was also observed in transgenic mice compared to WT. HGF has been shown to regulate lymph vessel formation (100). Increases in blood and lymph vasculature contribute to tumor proliferation and metastasis.

To further understand key regulators of HGF induced angiogenesis, microarray analysis was completed on whole lung and tumor samples from HGF TG and WT mice. Analysis demonstrated an overwhelming reduction in expression of angiogenic related genes, such as the VEGF gene family. However, at 10 weeks of age, and in tumor samples, a few pro-angiogenic CXC chemokines were up-regulated greater than 2-fold in the transgenic mice. The two CXC chemokines with highest expression, *Cxcl1* and *Cxcl2*, are homologues of human IL-8. Interleukins, specifically IL-8 and IL-6, have been revealed as pro-angiogenic cytokines in many cancers including NSCLC (32, 33). HGF can promote the induction of IL-8 in NPC and lung adenocarcinoma cells (90, 91).

The results from studying this aspect of c-Met signaling, suggest HGF over-expression mainly affects continued enhancement of vascularization with down-regulation of other key angiogenic factors such as the VEGF genes. These results could be used to further explain resistance to anti-VEGF therapies, which are currently being tested in several cancers, including NSCLC (17, 19). Resistance to bevacizumab and sunitinib has already been linked to HGF/c-Met expression (19, 21). Our animal model could be further used to study VEGF-independent angiogenesis in the hopes of identifying novel anti-angiogenic and anti-tumorigenic targets.

C-Met when stimulated by its ligand, HGF, initiates signaling cascades which results in a variety of biological effects. More recent studies have shown that c-Met may also be stimulated via HGF-independent mechanisms. The second aspect of c-Met signaling in this paper was focused on a mechanism of ligand-independent activation, EGFR crosstalk. Previous experiments by our laboratory revealed that EGFR could induce c-Met activation 8 hours after EGFR ligand stimulation (80). This activation is extended up to 48 hours post EGF treatment. Moreover, this delayed activation of c-Met was necessary to achieve maximal induction of invasion and migration by EGFR (80). The EGFR and c-Met pathways activate similar downstream effector molecules such as Kras/ MAPK, PI3K/AKT, and STAT. EGFR may utilize c-Met to amplify its signal to their shared downstream effectors.

STAT3 is known to be activated immediately downstream of EGFR ligand stimulation, as well as, downstream of HGF activated c-Met. STAT3 is a transcription factor that plays key regulatory roles in pro-inflammatory cytokine release, and tumor cell motility, invasion and proliferation (107). STAT3 was identified as a potential mediator downstream of delayed c-Met signaling previously by our laboratory (80). In this study we confirmed STAT3 phosphorylation requires delayed c-Met activation. STAT3 demonstrated a biphasic model of activation when stimulated by EGF in NSCLC cell lines. Initial activation occurred within 5 minutes of stimulation and subsided by 2 hours. A second wave of activation appeared around 8 hours post treatment and was seen up to 48 hours. The delayed activation of STAT3 correlated with delayed c-Met phosphorylation seen previously (80). Inhibition of active c-Met at delayed time points with PHA665752 also blocked phosphorylation of STAT3 at similar time points. This confirms that delayed STAT3 activation requires EGFR-induced c-Met signaling.

Several mechanisms for growth factor activation of STAT3 have been reported. C-Src is one such mediator, which also demonstrates a biphasic phosphorylation pattern in response to EGF. However, inhibition of delayed phospho-Src by PP2 failed to impede activation of STAT3. Co-immunoprecipitation of c-Met and STAT3 at 8-24 hours post EGF treatment highly suggests c-Met directly activates STAT3. In HeLa cells, c-Met signaling from perinuclear compartments was required for sustained phosphorylation and nuclear translocation of STAT3 (107). It is possible that in NSCLC cells, c-Met when activated via EGFR signals from intracellular compartments, potentially interacting with and activating those molecules which play a minor role in canonical signaling from the plasma membrane.

In order to better understand c-Met signaling in lung cancer, further investigation is essential. Improved understanding of critical intermediates involving in two differing c-Met signaling cascades (dependent or independent of ligand) would be useful for identifying key targets for NSCLC therapy. Combinational studies have highlighted the need for targeting multiple RTK inputs at once. In gliobastoma multiforme, a cocktail inhibitor of EGFR, c-Met, and PDGFR is necessary to completely block survival signaling through the PI3K/Akt pathway (111). Another study illustrated that dual treatment with a VEGFR/PDGFR inhibitor, sunitinib, and c-Met inhibitor significantly repressed tumor growth compared to sunitinib treatment alone (19). Our laboratory has recently shown that the combination of EGFR and c-Met TKIs has a greater effect on blocking pathways responsible for xenograft tumor progression compare to single target therapy alone (80). The redundancy of growth factor pathways can limit the efficacy of single agent angiogenic treatments. Thus, by further studying HGF/c-Met promotion of VEGF-independent angiogenesis, and EGFR-stimulated c-Met activation, we can identify ideal targets for inhibition of multiple pathways or combination therapy in NSCLC.

APPENDIX A

TABLE 5

Table 5. Genes with insignificant expression changes.

	HGF WT		HGF TG			
Symbol	**Avg Delta Ct**	**STD**	**Avg Delta Ct**	**STD**	**Fold Change**	***p***
10 week						
Csf3	-1.60	10.35	5.74	11.19	0.01	0.571
F2	1.47	9.29	8.63	0.61	0.01	0.286
Ereg	2.76	8.26	7.81	2.22	0.03	0.286
Hand2	10.17	2.88	13.28	2.10	0.12	0.272
Col18a1	4.36	0.38	6.98	2.62	0.16	0.101
Bai1	11.33	1.06	12.88	2.15	0.34	0.466
Timp1	12.04	0.65	13.29	2.13	0.42	0.917
Efnb2	-1.68	1.11	-0.45	0.82	0.43	0.117
Vegfa	0.19	0.44	1.37	0.82	0.44	0.073
Anpep	4.29	0.07	5.32	1.02	0.49	0.153
Plxdc1	5.57	0.31	6.58	1.04	0.50	0.241
S1pr1	-0.30	0.52	0.67	1.18	0.51	0.172
Figf	-0.98	0.66	-0.03	0.85	0.52	0.142
Plg	9.37	0.24	10.27	4.04	0.54	0.469
Thbs1	-0.44	0.84	0.35	1.15	0.58	0.370
Vegfb	3.79	0.23	4.53	0.59	0.60	0.084
Tbx1	2.17	0.24	2.88	1.17	0.61	0.436
Nrp1	-2.31	0.82	-1.70	0.28	0.66	0.153
Tgfa	4.28	0.74	4.87	0.95	0.67	0.341
Fzd5	2.10	0.80	2.62	0.65	0.70	0.321
Thbs2	5.81	1.15	6.32	3.63	0.70	0.524
Tnfaip2	2.60	1.29	3.11	0.40	0.71	0.336
Jag1	2.61	0.74	3.09	0.92	0.72	0.454
Tek	-2.10	0.76	-1.64	0.29	0.73	0.210
Tgfb3	4.45	0.33	4.84	0.69	0.76	0.406
Ctgf	-1.98	0.75	-1.62	0.40	0.78	0.385
Tmprss6	8.87	0.42	9.21	1.08	0.79	0.878

Table 5 Continued…

	HGF WT		HGF TG			
Symbol	**Avg Delta Ct**	**STD**	**Avg Delta Ct**	**STD**	**Fold Change**	***p***
Serpinf1	1.74	0.57	2.00	0.28	0.84	0.373
Itgb3	3.76	0.18	3.98	0.75	0.86	0.881
Gna13	0.30	1.29	0.48	0.65	0.88	0.540
Efna1	1.85	0.14	1.89	0.35	0.97	0.961
Vegfc	1.48	1.05	1.47	0.27	1.01	0.694
Fgf6	9.02	0.67	8.89	1.26	1.10	0.642
Angpt2	1.94	0.63	1.73	0.30	1.16	0.652
Mdk	3.59	0.30	3.37	0.14	1.17	0.250
Ifng	8.15	0.51	7.91	1.40	1.18	0.445
Mmp19	5.31	0.44	4.83	1.33	1.40	0.487
Smad5	0.72	0.86	0.14	0.33	1.49	0.284
Itgav	2.38	1.31	1.74	0.49	1.56	0.496
Tgfbr1	4.60	1.59	3.94	0.26	1.58	0.630
Egf	7.73	1.33	6.97	1.58	1.69	0.482
Fgf1	0.82	0.95	0.02	0.43	1.74	0.159
Hif1a	0.42	1.40	-0.61	0.62	2.03	0.242
Fgf2	2.93	1.44	1.91	0.97	2.04	0.393
Tnf	7.96	0.99	6.91	0.76	2.07	0.218
Igf1	3.30	1.68	2.04	0.71	2.39	0.259
Il6	8.43	1.13	7.00	1.17	2.70	0.165
Hgf	2.36	1.90	0.90	0.36	2.76	0.105
Lep	8.37	0.71	6.88	0.88	2.80	0.133
Angpt1	1.85	2.10	0.30	0.23	2.93	0.099
Ccl2	7.30	1.05	5.50	0.75	3.48	0.067
Cxcl1	6.82	1.17	4.78	1.15	4.11	0.175
Ccl11	5.09	0.58	3.02	0.95	4.20	0.086
Pgf	-1.34	3.67	-3.66	4.05	4.98	0.464
Cxcl2	6.02	1.16	3.62	1.32	5.31	0.233
Lect1	9.62	2.27	6.81	4.35	7.02	0.436
Tymp	5.04	0.56	0.06	4.22	31.63	0.367
	Avg	**STD**	**Avg**	**STD**	**Ratio (TG:WT)**	***p***
40 week						
Tnfrsf25	0.44	0.16	0.09	0.01	0.21	0.097
Cd44	0.71	0.25	0.16	0.09	0.22	0.098
Pik3c2a	0.41	0.18	0.09	0.02	0.22	0.132
Fos	0.59	0.24	0.14	0.09	0.23	0.127
Ncam1	0.47	0.23	0.11	0.03	0.24	0.163
Fas	0.52	0.35	0.14	0.09	0.27	0.274
Nfkb1	0.82	0.11	0.23	0.16	0.28	0.051
Casp8	0.30	0.21	0.09	0.02	0.29	0.292
Map2k1	0.56	0.26	0.16	0.12	0.29	0.191
Rasa1	0.33	0.23	0.10	0.03	0.29	0.293
S100a4	0.68	0.26	0.20	0.09	0.29	0.131
Rb1	0.54	0.25	0.16	0.06	0.30	0.175
Serpine1	0.90	0.04	0.28	0.26	0.31	0.077

Table 5 Continued…

	HGF WT		HGF TG			
Symbol	**Avg Delta Ct**	**STD**	**Avg Delta Ct**	**STD**	**Fold Change**	***p***
Cd82	0.28	0.11	0.09	0.02	0.31	0.138
Icam1	0.55	0.38	0.18	0.13	0.32	0.316
MMP9	0.25	0.15	0.08	0.01	0.34	0.025
Akt2	0.31	0.10	0.11	0.05	0.34	0.109
Myc	0.22	0.12	0.08	0.01	0.34	0.227
Jun	0.78	0.23	0.27	0.16	0.34	0.124
Itgb1	0.27	0.19	0.09	0.04	0.35	0.331
Ccl2	0.31	0.36	0.11	0.03	0.35	0.316
Cdc25a	0.26	0.17	0.09	0.03	0.36	0.306
Mdm2	0.20	0.14	0.07	0.01	0.36	0.334
Mcam	0.79	0.17	0.30	0.20	0.38	0.121
Hgf	0.22	0.19	0.08	0.04	0.38	0.120
Ets2	0.20	0.14	0.08	0.01	0.38	0.346
Gzma	0.17	0.12	0.07	0.01	0.39	0.333
Cxcl2	0.43	0.38	0.17	0.16	0.40	0.131
Plaur	0.21	0.07	0.08	0.02	0.40	0.125
Raf1	0.19	0.07	0.08	0.02	0.40	0.142
Nme4	0.21	0.06	0.09	0.02	0.41	0.102
Egfr	0.16	0.05	0.07	0.00	0.44	0.112
Casp9	0.51	0.26	0.22	0.17	0.44	0.323
MMP2	0.29	0.06	0.13	0.05	0.44	0.000
Erbb2	0.15	0.06	0.07	0.00	0.44	0.199
Cxcl1	0.22	0.25	0.10	0.05	0.45	0.302
Npr1	0.38	0.14	0.18	0.11	0.46	0.061
Ephb4	0.44	0.14	0.20	0.19	0.46	0.090
Pdgfb	0.30	0.32	0.14	0.10	0.47	0.281
Ccnd1	0.23	0.10	0.11	0.05	0.47	0.267
Hif1a	0.17	0.09	0.08	0.03	0.48	0.072
Il6	0.15	0.13	0.08	0.01	0.50	0.283
Serpinb2	0.13	0.06	0.07	0.00	0.51	0.279
Nudt6	0.26	0.12	0.13	0.06	0.51	0.100
Cdkn1a	0.17	0.02	0.09	0.02	0.52	0.062
Serpinb5	0.12	0.02	0.06	0.00	0.52	0.072
Ccl11	0.18	0.14	0.09	0.02	0.52	0.200
Cdh1	0.12	0.08	0.06	0.00	0.52	0.417
Cdkn1b	0.12	0.05	0.06	0.00	0.52	0.219
Mta2	0.13	0.05	0.07	0.00	0.52	0.206
Mta1	0.13	0.04	0.07	0.00	0.53	0.143
Mdk	0.21	0.05	0.11	0.03	0.53	0.011
Efna3	0.14	0.08	0.08	0.02	0.53	0.183
Mapk14	0.89	0.10	0.48	0.35	0.54	0.021
Met	0.12	0.05	0.07	0.00	0.56	0.240
Prkdc	0.12	0.02	0.07	0.00	0.57	0.076
Pten	0.11	0.05	0.07	0.01	0.57	0.053
Notch4	0.27	0.13	0.16	0.13	0.57	0.251

Table 5 Continued…

	HGF WT		HGF TG			
Symbol	**Avg Delta Ct**	**STD**	**Avg Delta Ct**	**STD**	**Fold Change**	***p***
Anpep	0.11	0.03	0.07	0.02	0.58	0.034
Muc1	0.12	0.03	0.07	0.00	0.58	0.134
Efnb2	0.75	0.11	0.44	0.33	0.59	0.125
Cflar	0.10	0.04	0.06	0.00	0.60	0.272
Tbx1	0.23	0.09	0.14	0.08	0.60	0.185
Itga3	0.10	0.04	0.06	0.00	0.61	0.301
Src	0.11	0.02	0.07	0.00	0.61	0.111
Wasf2	0.26	0.08	0.16	0.09	0.62	0.140
Mtss1	0.11	0.03	0.06	0.00	0.62	0.156
Ccne1	0.10	0.04	0.06	0.00	0.62	0.286
Twist1	0.10	0.02	0.07	0.00	0.63	0.101
Sphk1	0.68	0.15	0.43	0.34	0.63	0.224
Trp53	0.10	0.02	0.06	0.00	0.64	0.162
Lep	0.12	0.05	0.08	0.01	0.64	0.139
Ecgf1	0.16	0.04	0.10	0.06	0.64	0.162
Ifng	0.10	0.04	0.06	0.01	0.64	0.112
Timp2	0.42	0.21	0.27	0.23	0.65	0.382
Prok2	0.11	0.04	0.07	0.00	0.65	0.093
Itgb5	0.10	0.03	0.06	0.00	0.65	0.246
Pgf	0.10	0.04	0.06	0.01	0.65	0.147
Angpt2	0.19	0.05	0.12	0.07	0.65	0.187
Stab2	0.10	0.04	0.07	0.01	0.65	0.164
Tmprss6	0.10	0.04	0.06	0.01	0.66	0.121
Il10	0.13	0.03	0.08	0.03	0.66	0.088
Pecam1	0.12	0.05	0.08	0.01	0.67	0.171
Epas1	0.09	0.05	0.06	0.01	0.67	0.284
Tgfb1	0.13	0.06	0.09	0.02	0.68	0.144
Ptn	0.36	0.30	0.25	0.10	0.68	0.489
Cxcl10	0.09	0.03	0.07	0.01	0.69	0.161
Cdh5	0.09	0.04	0.06	0.01	0.70	0.259
Ctgf	0.96	0.05	0.67	0.31	0.70	0.112
Ifna1	0.08	0.04	0.06	0.01	0.70	0.191
Lect1	0.09	0.04	0.07	0.02	0.71	0.246
Tnfaip2	0.10	0.02	0.07	0.02	0.72	0.066
Fgf6	0.08	0.02	0.06	0.01	0.72	0.137
Edg1	0.96	0.05	0.69	0.25	0.72	0.079
Plg	0.13	0.02	0.09	0.02	0.72	0.077
Itgb3	0.10	0.05	0.07	0.02	0.73	0.156
Jag1	0.16	0.05	0.12	0.06	0.73	0.293
Hand2	0.09	0.03	0.06	0.01	0.74	0.249
Cxcl11	0.08	0.03	0.06	0.01	0.74	0.260
Cxcl5	0.08	0.02	0.06	0.01	0.74	0.118
TEK	0.87	0.10	0.65	0.28	0.75	0.099
Il12a	0.95	0.05	0.72	0.35	0.76	0.241
Smad5	0.09	0.03	0.07	0.00	0.76	0.184

Table 5 Continued…

	HGF WT		HGF TG			
Symbol	**Avg Delta Ct**	**STD**	**Avg Delta Ct**	**STD**	**Fold Change**	***p***
Tnnt1	0.09	0.02	0.07	0.00	0.76	0.072
Gna13	0.08	0.02	0.06	0.02	0.77	0.210
Angptl3	0.08	0.02	0.06	0.01	0.77	0.210
Nppb	0.08	0.01	0.06	0.01	0.78	0.105
Tgfbr1	0.09	0.02	0.07	0.02	0.78	0.049
Thbs1	0.09	0.02	0.07	0.02	0.78	0.096
Timp1	0.09	0.02	0.07	0.01	0.78	0.157
Il1b	0.76	0.31	0.59	0.15	0.78	0.382
Ptgs1	0.95	0.05	0.75	0.21	0.79	0.109
F2	0.07	0.02	0.06	0.01	0.79	0.277
Bai1	0.19	0.19	0.15	0.11	0.79	0.617
Egf	0.10	0.03	0.08	0.03	0.80	0.220
Mmp19	0.08	0.02	0.06	0.01	0.80	0.184
Ereg	0.07	0.02	0.05	0.02	0.80	0.266
Tnfsf12	0.08	0.02	0.06	0.01	0.81	0.166
Tnfsf15	0.08	0.02	0.06	0.01	0.81	0.237
Stab1	0.07	0.02	0.06	0.01	0.81	0.284
Lama5	0.09	0.02	0.07	0.02	0.82	0.389
Fgfr3	0.07	0.02	0.06	0.01	0.83	0.377
ItgaV	0.09	0.03	0.07	0.02	0.83	0.279
Kdr	0.11	0.03	0.09	0.04	0.84	0.508
Tbx4	0.08	0.02	0.07	0.00	0.84	0.231
Fgf2	0.08	0.02	0.07	0.02	0.86	0.270
Il18	0.87	0.10	0.75	0.16	0.86	0.249
Fzd5	0.06	0.02	0.06	0.02	0.87	0.530
Adra2b	0.20	0.07	0.18	0.08	0.87	0.617
Sh2d2a	0.07	0.02	0.06	0.01	0.87	0.384
Angpt1	0.08	0.02	0.07	0.02	0.90	0.503
Tgfb2	0.08	0.02	0.07	0.01	0.92	0.587
Serpinf1	0.08	0.02	0.08	0.02	0.94	0.774

PUBLICATIONS

Henry C, Lopez-Chavez A, Stabile LP, and Siegfried JM. HGF airway over-expression leads to enhanced pulmonary vascularization without induction of VEGF. Current Angiogenesis. 2012; 1: 52-63.

Siegfried JM, Gubish CT, Rothstein ME, Henry C, and Stabile LP. Combining the multitargeted tyrosine kinase inhibitor vandetanib with the antiestrogen fulvestrant enhances its antitumor effect in non-small cell lung cancer. J Thorac Oncol. 2012; 7: 485-95.

Dulak AM, Gubish CT, Stabile LP, Henry C, Siegfried JM. HGF-independent potentiation of EGFR action of c-Met. Oncogene. 2011; 30: 3625-35.

Guoqing H, Stabile LP, Yan Lui V, Gubish CT, Thomas SM, Joyce S, Henry C, Quesnelle K, Siegfried JM, Grandis JR. c-Src activation mediates EGFR inhibitor resistance in head and neck cancer through c-Met activation. In process.

BIBLIOGRAPHY

1. WHO. World Health Statistics Report. Geneva, Switzerland: World Health Organization; 2009. p. 47-51.

2. AmericanCancerSociety. Cancer Facts & Figures 2012. Atlanta: American Cancer Society; 2012.

3. AmericanLungAssociation. Trends in Tobacco Use. American Lung Association; 2011.

4. WHO Department of Gender WaH. Gender and tobacco control: A policy brief. Geneva, Switzerland: World Health Organization; 2007.

5. Wingo PA, Ries LA, Giovino GA, et al. Annual report to the nation on the status of cancer, 1973-1996, with a special section on lung cancer and tobacco smoking. J Natl Cancer Inst 1999; 91: 675-90.

6. Tung YH, Ko JL, Liang YF, Yin L, Pu Y, Lin P. Cooking oil fume-induced cytokine expression and oxidative stress in human lung epithelial cells. Environ Res 2001; 87: 47-54.

7. Zang EA, Wynder EL. Differences in lung cancer risk between men and women: examination of the evidence. J Natl Cancer Inst 1996; 88: 183-92.

8. Aberle DR, Adams AM, Berg CD, et al. Reduced lung-cancer mortality with low-dose computed tomographic screening. N Engl J Med; 365: 395-409.

9. Ohe Y. Chemoradiotherapy for lung cancer: current status and perspectives. Int J Clin Oncol 2004; 9: 435-43.

10. Aaronson SA. Growth factors and cancer. Science 1991; 254: 1146-53.

11. Siegfried JM, Gubish CT, Rothstein ME, Queiroz de Oliveira PE, Stabile LP. Signaling pathways involved in cyclooxygenase-2 induction by hepatocyte growth factor in non small-cell lung cancer. Mol Pharmacol 2007; 72: 769-79.

12. Hodkinson PS, Mackinnon A, Sethi T. Targeting growth factors in lung cancer. Chest 2008; 133: 1209-16.

13. Meert AP, Paesmans M, Martin B, et al. The role of microvessel density on the survival of patients with lung cancer: a systematic review of the literature with meta-analysis. Br J Cancer 2002; 87: 694-701.

14. Kreuter M, Kropff M, Fischaleck A, et al. Prognostic relevance of angiogenesis in stage III NSCLC receiving multimodality treatment. Eur Respir J 2009; 33: 1383-8.

15. Kadota K, Huang CL, Liu D, et al. The clinical significance of lymphangiogenesis and angiogenesis in non-small cell lung cancer patients. Eur J Cancer 2008; 44: 1057-67.

16. Mineo TC, Ambrogi V, Baldi A, et al. Prognostic impact of VEGF, CD31, CD34, and CD105 expression and tumour vessel invasion after radical surgery for IB-IIA non-small cell lung cancer. J Clin Pathol 2004; 57: 591-7.

17. Sandler A, Gray R, Perry MC, et al. Paclitaxel-carboplatin alone or with bevacizumab for non-small-cell lung cancer. N Engl J Med 2006; 355: 2542-50.

18. Salgia R. Prognostic significance of angiogenesis and angiogenic growth factors in nonsmall cell lung cancer. Cancer 2011; 117: 3889-99.

19. Shojaei F, Lee JH, Simmons BH, et al. HGF/c-Met acts as an alternative angiogenic pathway in sunitinib-resistant tumors. Cancer Res 2010; 70: 10090-100.

20. Sengupta S, Gherardi E, Sellers LA, Wood JM, Sasisekharan R, Fan TPD. Hepatocyte growth factor/scatter factor can induce angiogenesis independently of vascular endothelial growth factor. Arteriosclerosis Thrombosis and Vascular Biology 2003; 23: 69-75.

21. Kopetz S, Hoff PM, Morris JS, et al. Phase II trial of infusional fluorouracil, irinotecan, and bevacizumab for metastatic colorectal cancer: efficacy and circulating angiogenic biomarkers associated with therapeutic resistance. J Clin Oncol 2010; 28: 453-9.

22. Smith LA, Paszkiewicz GM, Hutson AD, Pauly JL. Inflammatory response of lung macrophages and epithelial cells to tobacco smoke: a literature review of ex vivo investigations. Immunol Res; 46: 94-126.

23. Jackson JR, Seed MP, Kircher CH, Willoughby DA, Winkler JD. The codependence of angiogenesis and chronic inflammation. FASEB J 1997; 11: 457-65.

24. Mukaida N. Pathophysiological roles of interleukin-8/CXCL8 in pulmonary diseases. Am J Physiol Lung Cell Mol Physiol 2003; 284: L566-77.

25. Acker FA, Voss HP, Timmerman H. Chemokines: structure, receptors and functions. A new target for inflammation and asthma therapy? Mediators Inflamm 1996; 5: 393-416.

26. Keeley EC, Mehrad B, Strieter RM. Chemokines as mediators of neovascularization. Arterioscler Thromb Vasc Biol 2008; 28: 1928-36.

27. Addison CL, Daniel TO, Burdick MD, et al. The CXC chemokine receptor 2, CXCR2, is the putative receptor for ELR+ CXC chemokine-induced angiogenic activity. J Immunol 2000; 165: 5269-77.

28. Heidemann J, Ogawa H, Dwinell MB, et al. Angiogenic effects of interleukin 8 (CXCL8) in human intestinal microvascular endothelial cells are mediated by CXCR2. J Biol Chem 2003; 278: 8508-15.

29. Strieter RM, Belperio JA, Burdick MD, Sharma S, Dubinett SM, Keane MP. CXC chemokines: angiogenesis, immunoangiostasis, and metastases in lung cancer. Ann N Y Acad Sci 2004; 1028: 351-60.

30. Keane MP, Belperio JA, Xue YY, Burdick MD, Strieter RM. Depletion of CXCR2 inhibits tumor growth and angiogenesis in a murine model of lung cancer. J Immunol 2004; 172: 2853-60.

31. Arenberg DA, Kunkel SL, Polverini PJ, Glass M, Burdick MD, Strieter RM. Inhibition of interleukin-8 reduces tumorigenesis of human non-small cell lung cancer in SCID mice. J Clin Invest 1996; 97: 2792-802.

32. Pold M, Zhu LX, Sharma S, et al. Cyclooxygenase-2-dependent expression of angiogenic CXC chemokines ENA-78/CXC Ligand (CXCL) 5 and interleukin-8/CXCL8 in human non-small cell lung cancer. Cancer Res 2004; 64: 1853-60.

33. Sun H, Chung WC, Ryu SH, et al. Cyclic AMP-responsive element binding protein- and nuclear factor-kappaB-regulated CXC chemokine gene expression in lung carcinogenesis. Cancer Prev Res (Phila Pa) 2008; 1: 316-28.

34. Luppi F, Longo AM, de Boer WI, Rabe KF, Hiemstra PS. Interleukin-8 stimulates cell proliferation in non-small cell lung cancer through epidermal growth factor receptor transactivation. Lung Cancer 2007; 56: 25-33.

35. Zhu YM, Webster SJ, Flower D, Woll PJ. Interleukin-8/CXCL8 is a growth factor for human lung cancer cells. Br J Cancer 2004; 91: 1970-6.

36. Zhu YM, Woll PJ. Mitogenic effects of interleukin-8/CXCL8 on cancer cells. Future Oncol 2005; 1: 699-704.

37. Dong G, Chen Z, Li ZY, Yeh NT, Bancroft CC, Van Waes C. Hepatocyte growth factor/scatter factor-induced activation of MEK and PI3K signal pathways contributes to expression of proangiogenic cytokines interleukin-8 and vascular endothelial growth factor in head and neck squamous cell carcinoma. Cancer Res 2001; 61: 5911-8.

38. Saffiotti U. Respiratory tract carcinogenesis by mineral fibres and dusts: models and mechanisms. Monaldi Arch Chest Dis 1998; 53: 160-7.

39. Wong HL, de Boer RH. Vandetanib for the treatment of non-small-cell lung cancer. Expert Opin Pharmacother; 12: 2271-8.

40. Kosaka T, Yatabe Y, Endoh H, Kuwano H, Takahashi T, Mitsudomi T. Mutations of the epidermal growth factor receptor gene in lung cancer: biological and clinical implications. Cancer Res 2004; 64: 8919-23.

41. Toyooka S, Mitsudomi T, Soh J, et al. Molecular oncology of lung cancer. Gen Thorac Cardiovasc Surg; 59: 527-37.

42. Li AR, Chitale D, Riely GJ, et al. EGFR mutations in lung adenocarcinomas: clinical testing experience and relationship to EGFR gene copy number and immunohistochemical expression. J Mol Diagn 2008; 10: 242-8.

43. Yarden Y. The EGFR family and its ligands in human cancer. signalling mechanisms and therapeutic opportunities. Eur J Cancer 2001; 37 Suppl 4: S3-8.

44. Engelman JA, Cantley LC. The role of the ErbB family members in non-small cell lung cancers sensitive to epidermal growth factor receptor kinase inhibitors. Clin Cancer Res 2006; 12: 4372s-6s.

45. Scaltriti M, Baselga J. The epidermal growth factor receptor pathway: a model for targeted therapy. Clin Cancer Res 2006; 12: 5268-72.

46. Stella GM, Luisetti M, Inghilleri S, et al. Targeting EGFR in non-small-cell lung cancer: lessons, experiences, strategies. Respir Med 2012; 106: 173-83.

47. Chattopadhyay A, Vecchi M, Ji Q, Mernaugh R, Carpenter G. The role of individual SH2 domains in mediating association of phospholipase C-gamma1 with the activated EGF receptor. J Biol Chem 1999; 274: 26091-7.

48. Janku F, Garrido-Laguna I, Petruzelka LB, Stewart DJ, Kurzrock R. Novel therapeutic targets in non-small cell lung cancer. J Thorac Oncol; 6: 1601-12.

49. Wu CC, Hsu HY, Liu HP, et al. Reversed mutation rates of KRAS and EGFR genes in adenocarcinoma of the lung in Taiwan and their implications. Cancer 2008; 113: 3199-208.

50. Eberhard DA, Johnson BE, Amler LC, et al. Mutations in the epidermal growth factor receptor and in KRAS are predictive and prognostic indicators in patients with non-small-cell lung cancer treated with chemotherapy alone and in combination with erlotinib. J Clin Oncol 2005; 23: 5900-9.

51. Engelman JA, Zejnullahu K, Mitsudomi T, et al. MET amplification leads to gefitinib resistance in lung cancer by activating ERBB3 signaling. Science 2007; 316: 1039-43.

52. Ma PC, Maulik G, Christensen J, Salgia R. c-Met: structure, functions and potential for therapeutic inhibition. Cancer Metastasis Rev 2003; 22: 309-25.

53. Stoker M, Gherardi E, Perryman M, Gray J. Scatter factor is a fibroblast-derived modulator of epithelial cell mobility. Nature 1987; 327: 239-42.

54. Mars WM, Zarnegar R, Michalopoulos GK. Activation of hepatocyte growth factor by the plasminogen activators uPA and tPA. Am J Pathol 1993; 143: 949-58.

55. Ponzetto C, Bardelli A, Zhen Z, et al. A multifunctional docking site mediates signaling and transformation by the hepatocyte growth factor/scatter factor receptor family. Cell 1994; 77: 261-71.

56. Peschard P, Fournier TM, Lamorte L, et al. Mutation of the c-Cbl TKB domain binding site on the Met receptor tyrosine kinase converts it into a transforming protein. Mol Cell 2001; 8: 995-1004.

57. Meloche S, Pouyssegur J. The ERK1/2 mitogen-activated protein kinase pathway as a master regulator of the G1- to S-phase transition. Oncogene 2007; 26: 3227-39.

58. Rivat C, De Wever O, Bruyneel E, Mareel M, Gespach C, Attoub S. Disruption of STAT3 signaling leads to tumor cell invasion through alterations of homotypic cell-cell adhesion complexes. Oncogene 2004; 23: 3317-27.

59. Galimi F, Cottone E, Vigna E, et al. Hepatocyte growth factor is a regulator of monocyte-macrophage function. J Immunol 2001; 166: 1241-7.

60. Birchmeier C, Gherardi E. Developmental roles of HGF/SF and its receptor, the c-Met tyrosine kinase. Trends Cell Biol 1998; 8: 404-10.

61. Schmidt C, Bladt F, Goedecke S, et al. Scatter factor/hepatocyte growth factor is essential for liver development. Nature 1995; 373: 699-702.

62. Liu X, Yao W, Newton RC, Scherle PA. Targeting the c-MET signaling pathway for cancer therapy. Expert Opin Investig Drugs 2008; 17: 997-1011.

63. Michalopoulos GK, DeFrances MC. Liver regeneration. Science 1997; 276: 60-6.

64. Nakamura T, Mizuno S, Matsumoto K, Sawa Y, Matsuda H. Myocardial protection from ischemia/reperfusion injury by endogenous and exogenous HGF. J Clin Invest 2000; 106: 1511-9.

65. Sato T, Tani Y, Murao S, et al. Focal enhancement of expression of c-Met/hepatocyte growth factor receptor in the myocardium in human myocardial infarction. Cardiovasc Pathol 2001; 10: 235-40.

66. Yi S, Chen JR, Viallet J, Schwall RH, Nakamura T, Tsao MS. Paracrine effects of hepatocyte growth factor/scatter factor on non-small-cell lung carcinoma cell lines. Br J Cancer 1998; 77: 2162-70.

67. Harvey P, Warn A, Newman P, Perry LJ, Ball RY, Warn RM. Immunoreactivity for hepatocyte growth factor scatter factor and its receptor, met, in human lung carcinomas and malignant mesotheliomas. J Pathol 1996; 180: 389-94.

68. Olivero M, Rizzo M, Madeddu R, et al. Overexpression and activation of hepatocyte growth factor scatter factor in human non-small-cell lung carcinomas. Br J Cancer 1996; 74: 1862-8.

69. Takanami I, Tanana F, Hashizume T, et al. Hepatocyte growth factor and c-met/hepatocyte growth factor receptor in pulmonary adenocarcinomas: An evaluation of their expression as prognostic markers. Oncology 1996; 53: 392-7.

70. Christensen JG, Burrows J, Salgia R. c-Met as a target for human cancer and characterization of inhibitors for therapeutic intervention. Cancer Lett 2005; 225: 1-26.

71. Jiang WG, Martin TA, Parr C, Davies G, Matsumoto K, Nakamura T. Hepatocyte growth factor, its receptor, and their potential value in cancer therapies. Critical Reviews in Oncology/Hematology 2005; 53: 35-69.

72. Sheen-Chen SM, Liu YW, Eng HL, Chou FF. Serum levels of hepatocyte growth factor in patients with breast cancer. Cancer Epidemiol Biomarkers Prev 2005; 14: 715-7.

73. Maulik G, Shrikhande A, Kijima T, Ma PC, Morrison PT, Salgia R. Role of the hepatocyte growth factor receptor, c-Met, in oncogenesis and potential for therapeutic inhibition. Cytokine Growth Factor Rev 2002; 13: 41-59.

74. Kong-Beltran M, Seshagiri S, Zha J, et al. Somatic mutations lead to an oncogenic deletion of met in lung cancer. Cancer Res 2006; 66: 283-9.

75. Lai AZ, Abella JV, Park M. Crosstalk in Met receptor oncogenesis. Trends Cell Biol 2009; 19: 542-51.

76. Wang R, Kobayashi R, Bishop JM. Cellular adherence elicits ligand-independent activation of the Met cell-surface receptor. Proc Natl Acad Sci U S A 1996; 93: 8425-30.

77. Conrotto P, Corso S, Gamberini S, Comoglio PM, Giordano S. Interplay between scatter factor receptors and B plexins controls invasive growth. Oncogene 2004; 23: 5131-7.

78. Fischer OM, Giordano S, Comoglio PM, Ullrich A. Reactive oxygen species mediate Met receptor transactivation by G protein-coupled receptors and the epidermal growth factor receptor in human carcinoma cells. J Biol Chem 2004; 279: 28970-8.

79. Jo M, Stolz DB, Esplen JE, Dorko K, Michalopoulos GK, Strom SC. Cross-talk between epidermal growth factor receptor and c-Met signal pathways in transformed cells. J Biol Chem 2000; 275: 8806-11.

80. Dulak AM, Gubish CT, Stabile LP, Henry C, Siegfried JM. HGF-independent potentiation of EGFR action by c-Met. Oncogene 2011; 30: 3625-35.

81. Stabile LP, Lyker JS, Huang L, Siegfried JM. Inhibition of human non-small cell lung tumors by a c-Met antisense/U6 expression plasmid strategy. Gene Ther 2004; 11: 325-35.

82. Stabile LP, Rothstein ME, Keohavong P, et al. Therapeutic targeting of human hepatocyte growth factor with a single neutralizing monoclonal antibody reduces lung tumorigenesis. Mol Cancer Ther 2008; 7: 1913-22.

83. Gherardi E, Birchmeier W, Birchmeier C, Vande Woude G. Targeting MET in cancer: rationale and progress. Nat Rev Cancer; 12: 89-103.

84. Karamouzis MV, Konstantinopoulos PA, Papavassiliou AG. Targeting MET as a strategy to overcome crosstalk-related resistance to EGFR inhibitors. Lancet Oncol 2009; 10: 709-17.

85. Shaw AT, Yeap BY, Mino-Kenudson M, et al. Clinical features and outcome of patients with non-small-cell lung cancer who harbor EML4-ALK. J Clin Oncol 2009; 27: 4247-53.

86. Stabile LP, Lyker JS, Land SR, Dacic S, Zamboni BA, Siegfried JM. Transgenic mice overexpressing hepatocyte growth factor in the airways show increased susceptibility to lung cancer. Carcinogenesis 2006; 27: 1547-55.

87. Siegfried JM, Krishnamachary N, Gaither Davis A, Gubish C, Hunt JD, Shriver SP. Evidence for autocrine actions of neuromedin B and gastrin-releasing peptide in non-small cell lung cancer. Pulm Pharmacol Ther 1999; 12: 291-302.

88. Folkman J. What is the evidence that tumors are angiogenesis dependent. J Natl Cancer Inst 1990; 82: 4-6.

89. Mattern J, Koomagi R, Volm M. Association of vascular endothelial growth factor expression with intratumoral microvessel density and tumour cell proliferation in human epidermoid lung carcinoma. Br J Cancer 1996; 73: 931-4.

90. Chiang YY. Hepatocyte growth factor induces hypoxia-related interleukin-8 expression in lung adenocarcinoma cells. Mol Carcinog 2009; 48: 662-70.

91. Xie LQ, Bian LJ, Li Z, Li Y, Liang YJ. Co-elevated expression of hepatocyte growth factor and Interleukin-8 contributes to poor prognosis of patients with primary nasopharyngeal carcinoma. Oncol Rep 2010; 23: 141-50.

92. Avraamides CJ, Garmy-Susini B, Varner JA. Integrins in angiogenesis and lymphangiogenesis. Nat Rev Cancer 2008; 8: 604-17.

93. Kajiya K, Hirakawa S, Ma B, Drinnenberg I, Detmar M. Hepatocyte growth factor promotes lymphatic vessel formation and function. EMBO J 2005; 24: 2885-95.

94. Lin EY, Pollard JW. Tumor-associated macrophages press the angiogenic switch in breast cancer. Cancer Res 2007; 67: 5064-6.

95. Nakamura Y, Matsubara D, Goto A, et al. Constitutive activation of c-Met is correlated with c-Met overexpression and dependent on cell-matrix adhesion in lung adenocarcinoma cell lines. Cancer Science 2008; 99: 14-22.

96. Birchmeier C, Birchmeier W, Gherardi E, Vande Woude GF. Met, metastasis, motility and more. Nat Rev Mol Cell Biol 2003; 4: 915-25.

97. Hungerford JE, Little CD. Developmental biology of the vascular smooth muscle cell: building a multilayered vessel wall. J Vasc Res 1999; 36: 2-27.

98. Helfrich I, Scheffrahn I, Bartling S, et al. Resistance to antiangiogenic therapy is directed by vascular phenotype, vessel stabilization, and maturation in malignant melanoma. J Exp Med 2010; 207: 491-503.

99. Nillesen ST, Geutjes PJ, Wismans R, Schalkwijk J, Daamen WF, van Kuppevelt TH. Increased angiogenesis and blood vessel maturation in acellular collagen-heparin scaffolds containing both FGF2 and VEGF. Biomaterials 2007; 28: 1123-31.

100. Cao R, Bjorndahl MA, Gallego MI, et al. Hepatocyte growth factor is a lymphangiogenic factor with an indirect mechanism of action. Blood 2006; 107: 3531-6.

101. Banerji S, Ni J, Wang SX, et al. LYVE-1, a new homologue of the CD44 glycoprotein, is a lymph-specific receptor for hyaluronan. J Cell Biol 1999; 144: 789-801.

102. Beasley NJ, Prevo R, Banerji S, et al. Intratumoral lymphangiogenesis and lymph node metastasis in head and neck cancer. Cancer Res 2002; 62: 1315-20.

103. Dadras SS, Paul T, Bertoncini J, et al. Tumor lymphangiogenesis: a novel prognostic indicator for cutaneous melanoma metastasis and survival. Am J Pathol 2003; 162: 1951-60.

104. Steins MB, Reinmuth N, Bischoff H, Kindermann M, Thomas M. Targeting the epidermal growth factor receptor in non-small cell lung cancer. Onkologie 2010; 33: 704-9.

105. Iivanainen E, Lauttia S, Zhang N, et al. The EGFR inhibitor gefitinib suppresses recruitment of pericytes and bone marrow-derived perivascular cells into tumor vessels. Microvasc Res 2009; 78: 278-85.

106. Hasina R, Whipple ME, Martin LE, Kuo WP, Ohno-Machado L, Lingen MW. Angiogenic heterogeneity in head and neck squamous cell carcinoma: biological and therapeutic implications. Lab Invest 2008; 88: 342-53.

107. Kermorgant S, Parker PJ. Receptor trafficking controls weak signal delivery: a strategy used by c-Met for STAT3 nuclear accumulation. J Cell Biol 2008; 182: 855-63.

108. Yu H, Pardoll D, Jove R. STATs in cancer inflammation and immunity: a leading role for STAT3. Nat Rev Cancer 2009; 9: 798-809.

109. Silva CM. Role of STATs as downstream signal transducers in Src family kinase-mediated tumorigenesis. Oncogene 2004; 23: 8017-23.

110. Boccaccio C, Ando M, Tamagnone L, et al. Induction of epithelial tubules by growth factor HGF depends on the STAT pathway. Nature 1998; 391: 285-8.

111. Stommel JM, Kimmelman AC, Ying H, et al. Coactivation of receptor tyrosine kinases affects the response of tumor cells to targeted therapies. Science 2007; 318: 287-90.